



How was the Carboniferous Balkhash–West Junggar remnant ocean filled and closed? Insights from the Well Tacan-1 strata in the Tacheng Basin, NW China



Di Li, Dengfa He ^{*}, Xuefeng Qi, Ningning Zhang

The Key Laboratory of Marine Reservoir Evolution and Hydrocarbon Accumulation Mechanism, The Ministry of Education, China University of Geosciences, Beijing 100083, China

ARTICLE INFO

Article history:

Received 29 April 2013

Received in revised form 4 October 2013

Accepted 4 October 2013

Available online 26 October 2013

Handling Editor: W.J. Xiao

Keywords:

Geochronology

Geochemistry

Tectonic–sedimentary evolution

Well Tacan-1

Tacheng Basin

ABSTRACT

The Balkhash–West Junggar remnant ocean is a conspicuous tectonic feature that had an important effect on the Paleozoic tectonic evolution of the Central Asian Orogenic Belt. How the Carboniferous Balkhash–West Junggar remnant ocean was filled and closed is poorly understood. In this study, we focus on the integrated tectonic–sedimentary evolution of the Tacheng Basin, which is located in the eastern part of the Balkhash–West Junggar remnant ocean, using high-resolution seismic reflection, well-line, geochronological and geochemical data to establish the filling of the basin by sediments and its evolution. The Carboniferous Balkhash–West Junggar remnant ocean basin was filled with Early Carboniferous deep marine mudstone and interbedded sandstone with minor andesite, basalt and tuff, and Late Carboniferous basalt, andesite, breccia and tuff and shallow marine mudstone and sandstone. The Carboniferous igneous assemblage mainly consists of basalt with high Nb content and $(Nb/La)_{PM}$ values and concomitant magnesian andesites with adakite geochemical characteristics of high Sr and low Y and Yb, suggesting a subduction-related tectonic setting. Zircons in the tuff that underlies the basalts and magnesian andesites were dated to ca. 315 Ma by LA-ICP-MS U-Pb. The identified unconformity between the Carboniferous and Lower Permian from seismic reflection profile in Well Tacan-1 subdivided the Carboniferous–Early Permian strata into two tectonostratigraphic units. The Lower Permian sequences overlap the Carboniferous strata and the facies transition from the submarine Carboniferous to the terrigenous Lower Permian indicates that the Balkhash–West Junggar remnant ocean closed during the Early Permian. These new data suggest that the sedimentary filling of the basin was in response to subduction and accretionary processes and that oceanic subduction was an important mechanism that led to the shrinking, filling and closure of the Balkhash–West Junggar remnant ocean because of compression. Therefore, lateral crust growth through subduction–accretionary processes still played an important role in the Carboniferous construction of western Junggar.

© 2013 International Association for Gondwana Research. Published by Elsevier B.V. All rights reserved.

1. Introduction

The Central Asian Orogenic Belt (CAOB) corresponds to the Altaiid tectonic collage by Sengör and coworkers (Sengör et al., 1993; Sengör and Natal'in, 1996) and is the world's largest Phanerozoic accretionary orogen. It is the product of the successive accretion and amalgamation of Precambrian continental blocks, ancient island arcs, accretionary complexes, ophiolites and passive continental margins since the Neoproterozoic (Sengör and Natal'in, 1996; Buslov et al., 2001; Badarch et al., 2002; Khain et al., 2002, 2003; Xiao et al., 2003; Dobretsov et al., 2004; Jahn et al., 2004; Safonova et al., 2004; Yakubchuk, 2004; Helo et al., 2006; Kröner et al., 2007; Windley et al., 2007; Xiao et al., 2009, 2010) (Fig. 1a). The western Junggar region, located at the eastern margin of the Kazakhstan orocline (Windley et al., 2007; Xiao et al., 2010) (Fig. 1b), has long been an important region for studying the evolution of the CAOB (Khain et al., 2002; Yakubchuk,

2004; Seltmann and Porter, 2005; Windley et al., 2007; Kröner et al., 2008; Santosh et al., 2009; Shen et al., 2009, 2010). Several belts of ophiolitic mélanges and subduction-related volcanic rocks with positive ε_{Nd} values contain evidence for the oceanic evolution from the Cambrian to Carboniferous (Zhang et al., 1995; Buckman and Aitchison, 2004), which constrains the long-lived accretion history without much involvement of ancient continental crust (Feng et al., 1989; Zhang et al., 1993; Jian et al., 2005; Zhu and Xu, 2006; Gu et al., 2009; Zhang and Guo, 2010; Li et al., 2012; Xu et al., 2012; He et al., 2013) and without the short amalgamation phases of multiple microcontinents (Mossakovskiy et al., 1993). Moreover, the extensive occurrence of Carboniferous adakites, high-Mg diorite dikes and charnockites in this area indicates that there may have been an oceanic island arc setting in the Carboniferous in western Junggar (Geng et al., 2009; Liu et al., 2009; Tang et al., 2009; Yin et al., 2010). Tectonic evolution models, such as a single subduction zone (Wang et al., 2003), arc–arc collisions (Feng et al., 1991; Zhang et al., 1995; Buckman and Aitchison, 2004) and oceanic-ridge subduction (Geng et al., 2009; Liu et al., 2009; Tang et al., 2009, 2010; Yin et al., 2010) have been proposed to explain the

* Corresponding author.

E-mail address: hedengfa282@263.net (D. He).

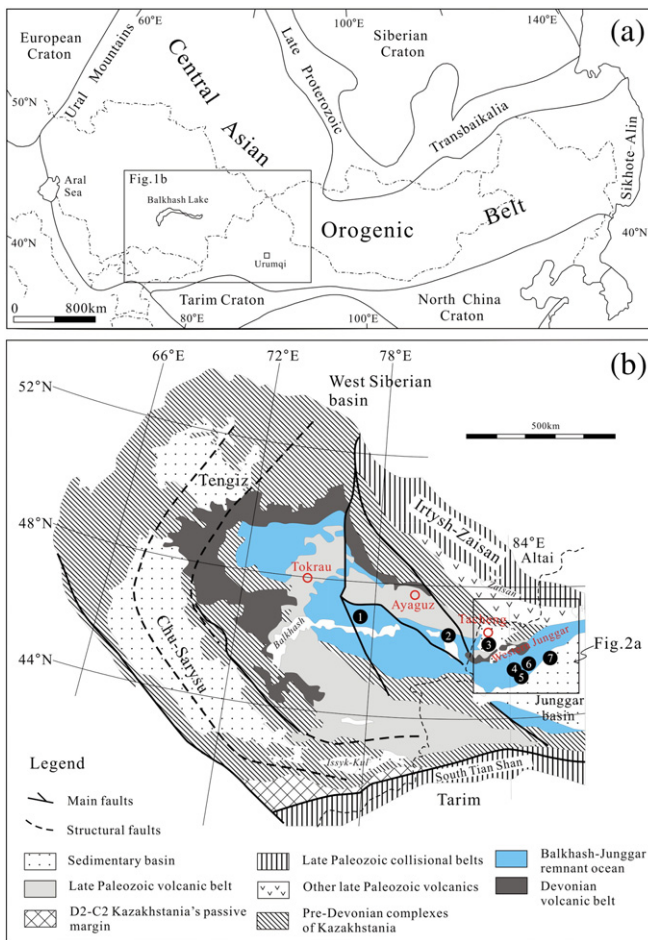


Fig. 1. (a) Location of the study area in the Central Asian Orogenic Belt. (b) Tectonic map showing the main units separated by the major suture zones in the West Junggar regions and adjacent Kazakhstan regions. The location of West Junggar is shown with a box. (c) Map of the Tacheng Basin showing the locations of Well Tacan-1 samples taken for major and trace element analyses and zircon U-Pb dating, and simplified tectonic lines. Numbers ①–⑦ show the localities of stratigraphic columns in Fig. 18. Data in panel (a) is modified after Jahn et al., 2004; Windley et al., 2007; Han et al., 2010. Data in panel (b) is modified after BGMRXUAR (1993); Windley et al., 2007.

evolution of the western Junggar region in the Carboniferous. The Balkhash area, located in the central Kazakhstan orocline and the westward extension of the western Junggar region, shares the same tectonic evolution history with the western Junggar region. The comparison of tectonic features proved the existence of a limited Carboniferous remnant oceanic basin that existed in the Balkhash–West Junggar region (He and Xu, 2003; He et al., 2004). The floor of the ocean basin was covered by marine lavas, peperite and sedimentary rocks (Li and Jin, 1989; Jin and Li, 1999; Guo et al., 2002). Recently, Chen et al. (2013) identified Late Devonian peperites at the base of the Tailegula Formation in the western Junggar, which further confirms the existence of a Carboniferous western Junggar remnant ocean basin. Latest Carboniferous–Middle Permian stitching plutons intruded the western Junggar accretionary complexes and adjacent parts of East Kazakhstan (Vladimirov et al., 2008; Kuibida et al., 2009). In addition, Early Permian bimodal volcanic rocks, A-type granites and molasses are present in western Junggar (Zhou et al., 2008; Chen et al., 2010). The data indicate that western Junggar had entered a post-collisional evolution stage during the Latest Carboniferous–Middle Permian (Han et al., 2006; Su et al., 2006; T.F. Zhou et al., 2006; Zhou et al., 2008; Chen et al., 2010) while the Balkhash–West Junggar remnant ocean basin disappeared in this period. The well-exposed Carboniferous strata in western Junggar provide an opportunity to unravel the accretionary processes spatially and temporally; however, few detailed data are reported that could

explain how the Carboniferous Balkhash–West Junggar remnant ocean filled and closed.

The Tacheng Basin, a link to the Balkhash and western Junggar remnant ocean, contains well-preserved volcanic–sedimentary sequences. Naturally, the fill material and tectonic setting are keys to understand the filling and evolution of the basin. The subsequent deformation, uplift, erosion and crustal growth in Central Asia modified the original tectonic framework; nonetheless, relatively well-developed sequences are preserved in this basin. Thus, these filling sequences are valuable records of the tectonic evolution of the accretionary orogen and the volcanic rocks can further constrain the tectonic evolution. To explore the tectonic–sedimentary evolution of the Balkhash–West Junggar remnant ocean basin, we conducted a comprehensive study of the Well Tacan-1 in the Tacheng Basin (Fig. 2a). The dataset, including high-resolution seismic reflection data and the relatively complete stratigraphic sequence provides critical information for unraveling the filling of the Balkhash–West Junggar remnant ocean. In addition, we carried out whole-rock and Sr–Nd isotope geochemistry and zircon U–Pb geochronological analysis of the Upper Carboniferous volcanic rocks to constrain the Carboniferous tectonic setting. The new results were combined with previously reported data to discuss the evolution of the sedimentary filling and the closing mechanism of the Balkhash–West Junggar remnant ocean basin.

2. Geological setting

The Balkhash–West Junggar remnant ocean occupies the central segment of the CAOB and extends E–W for more than 1000 km from Balkhash to western Junggar (Fig. 1b). It is surrounded by northern (Chingiz) and southern (North Tian shan) Paleozoic volcanic belts that contain Paleozoic ophiolites in the Balkhash and western Junggar regions (Zhao and He, 2013), indicating that they may have originated from the same paleo-oceanic tectonic setting. Therefore, the Balkhash and western Junggar remnant ocean had a similar evolution and filling history.

The western Junggar terrane is divided into northern and southern by the Xiemisitai fault. In the north, western Junggar terrane mainly consists of the Zharma–Saur and Boshchekul–Chingiz volcanic arcs and is characterized by E–W-trending faults and fault-bounded blocks (BGMRX, Bureau of Geology Mineral Resources of Xinjiang Uygur Autonomous Region, 1993; Fig. 2a). These arcs consist of Late Paleozoic tuff, tuffaceous limestone and sandstone and Early Paleozoic tuffaceous siltstone, tuffaceous sandstone and muddy siltstone, which are intruded by 304–263 Ma intermediate to felsic plutons (Han et al., 2006; Zhou et al., 2008; Chen et al., 2010; Shen et al., 2012). The plutons reflect the result of the southward subduction of the Irtish–Zaysan Ocean beneath the Kazakhstan block (Windley et al., 2007; Vladimirov et al., 2008). The southern western Junggar terrane, in contrast, consists of successive accretionary complexes separated by NE–SW oriented faults, such as the Darbut fault (Fig. 2a). These complexes consist of Devonian to Carboniferous sandstone and volcanic rocks, including basalt, andesitic basalt and andesite (BGMRX, Bureau of Geology Mineral Resources of Xinjiang Uygur Autonomous Region, 1993; Shen and Jin, 1993). They are intruded by alkali-feldspar granite batholiths and mafic dikes. The age of the granodioritic stocks is between 315 and 298 Ma (Chen et al., 2006; Han et al., 2006; Su et al., 2006; Geng et al., 2009; Tang et al., 2009; Yin et al., 2010; Tang et al., 2012a). The Carboniferous volcanic rocks in these accretionary complexes have SHRIMP and LA-ICP-MS U–Pb ages of 358–328 Ma (An and Zhu, 2009; Guo et al., 2010), which implies that the Late Carboniferous strata were denuded or had not formed. This may lead to misunderstanding of the Carboniferous tectonic environment of West Junggar (Coleman, 1989; Chen and Jahn, 2004; Han et al., 2006; Xiao et al., 2008; Geng et al., 2009, 2011). Therefore, much more geochemical work on the Late Carboniferous volcanic rocks is needed to clarify the source regions and tectonic setting.

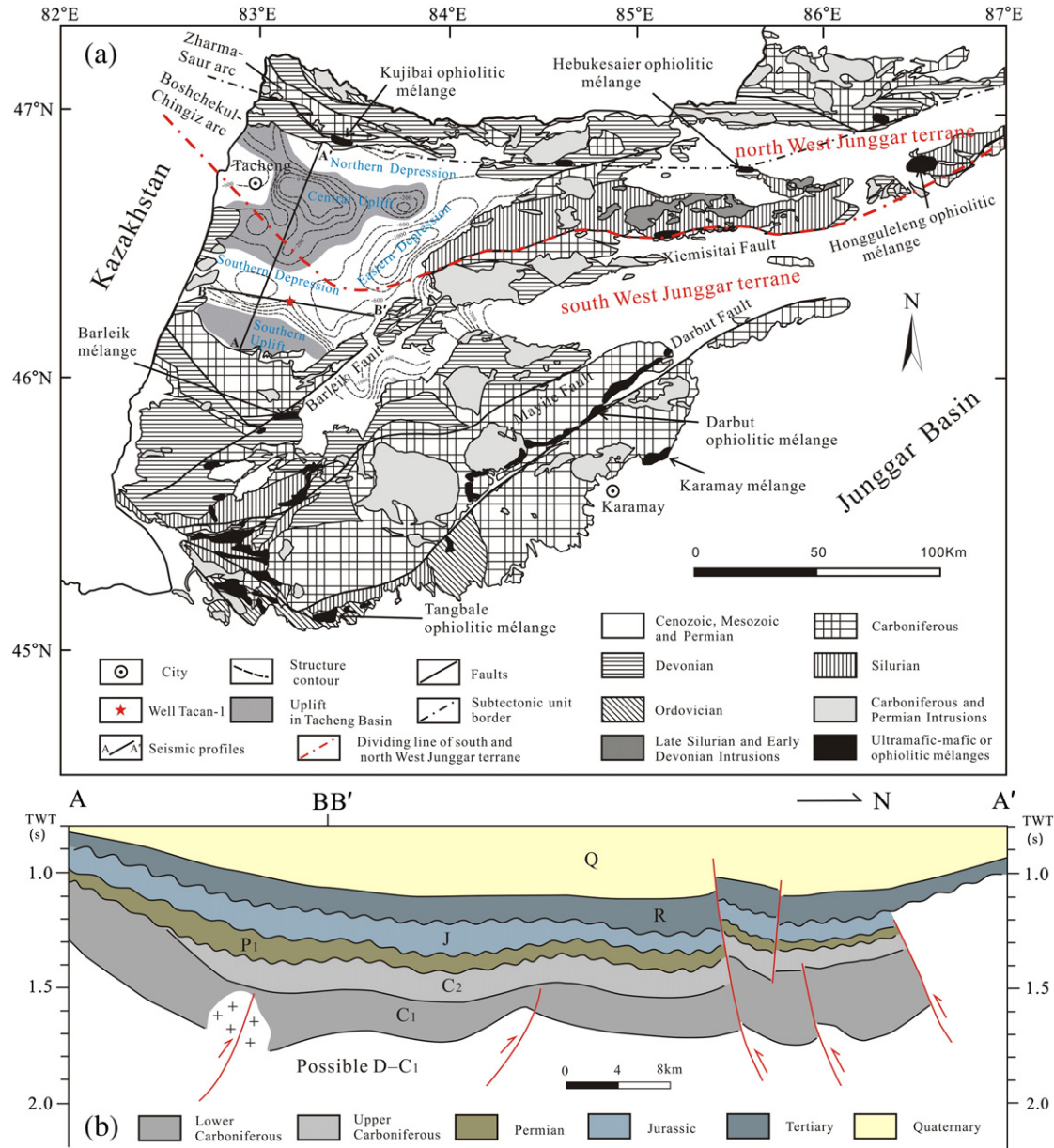


Fig. 2. South–North geological transect (BB') of the Tacheng Basin (after Xinjiang Oilfield Company). D—Devonian, C₁—Lower Carboniferous, C₂—Upper Carboniferous, P—Permian, J—Jurassic, R—Tertiary and the white area—Volcanic rocks.

Western Junggar is in the south of the Tacheng Basin and the Zharma-Saur Mountains are in the north. The sedimentary rocks of the basin range from Late Paleozoic to Cenozoic and experienced an extensional stage in Early Paleozoic and a convergence stage in Late Paleozoic (He et al., 1994). Tectonically, the northern part of the Tacheng Basin mainly involves the Zharma-Saur and Boshchekul-Chingiz volcanic arcs from north to south. Parts of the Boshchekul-Chingiz volcanic arc are covered by Meso-Cenozoic strata of the Tacheng Basin (Fig. 1b). The Zharma-Saur volcanic arc is separated by the Irtysh-Zaysan suture zone from the Altai orogen in the north and from the Boshchekul-Chingiz volcanic arc and Tacheng Basin by the Kujibai ophiolitic belts. The latter occur along large-scale E-W or NE-SW oriented faults and may extend eastward to the Hebukesaier and Hongguleleng ophiolitic belts. Devonian-Early Carboniferous plutons outcrop along both sides of the Irtysh-Zaysan suture zone and the intruding plutons have zircon U-Pb ages of 307–299 Ma (Kuibida et al., 2009), suggesting that suturing may have occurred in the Late Carboniferous (Buslov et al., 2001, 2004; Windley et al., 2007; Han et al.,

2010). The altered gabbros from the Kujibai ophiolite yielded a SHRIMP zircon U-Pb age of 478 Ma (Zhu and Xu, 2006), which is similar to the age of the Hongguleleng ophiolite (475 Ma, Jian et al., 2005) and together they may represent remnants of the Early Devonian interarc oceanic basin (Filippova et al., 2001). The age of the Barleik ophiolite in the southern part of the Tacheng Basin is considered Middle Devonian based on radiolarians in chert (Feng, 1987) and may be slices of another ophiolite separated and displaced by faulting (Buckman and Aitchison, 2004). The age of the Darbut ophiolite ranges from 303 to 426 Ma (Zhang and Huang, 1992; Gu et al., 2009; Liu et al., 2009; Chen and Zhu, 2011; Yang et al., 2012), demonstrating a complex accretionary history that even continued into the Late Carboniferous.

3. Stratigraphic successions and sample descriptions

The Tacheng Basin is located in the western part of the West Junggar region where the connected Chingiz arc and Junggar composite basin contain a 4 km thick Carboniferous–Cenozoic sedimentary

sequence. The basin is divided into four first-order tectonic units (Fig. 2a): the Central Uplift, the Southern Depression, the Eastern Depression and the Northern Depression. The Well Tacan-1 is located at the transitional zone of a strong–weak magnetic anomaly in the Southern Depression and mainly goes through Neogene (0–154 m), Paleogene (154–346 m), Jurassic (346–572 m), Lower Permian (Kalagang Formation, 572–940 m), Upper Carboniferous (Jimunai Formation, 940–2778 m) and part of Lower Carboniferous (Nanmingshui Formation, 2778–3300 m) (Fig. 2b). In general, a period of volcanic activity shows the cycle of a volcano from eruption to lava gushes. According to the eruption-and-gushing-out model, thirty-two periods of volcanic activity were identified in the Well Tacan-1. The mudstones at 790–810 m contain momosaccate pollen of *Florinites* and *Cordaitina*, suggesting an Early Permian age for the Kalagang Formation. Moreover, the mudstones at 1162–1176 m contain many pollen and spore assemblages of *Protohaploxylinu* and *Striatooabietites*. Some *Hamiapollenites*, monosaccate pollen, Costa pollen and Pteridophyta spores were also discovered. This assemblage of gymnosperm pollen and little fern spore did not contain Early Carboniferous pollen or spore assemblages. In contrast, the Early Carboniferous samples from North Xinjiang and the low content of *Cordaitina* and *Hamiapollenites* differ from that of the Middle-Late Permian, suggesting a Carboniferous age for the Jimunai Formation.

The nearly 2360 m thick Carboniferous formation in the Well Tacan-1 is at a depth of 940–3300 m, and includes the Upper Carboniferous Jimunai Formation (C_2) and the Lower Carboniferous Nanmingshui Formation (C_1) (Fig. 3). The Jimunai Formation mainly consists of basalt, volcanic breccia, tuff, andesite, rhyolite, conglomerate and mudstone. The Nanmingshui Formation mainly consists of dark gray andesite, tuff, mudstone and basalt. The contact between the Early and Late Carboniferous formations is conformable, whereas the Lower Permian series is unconformably overlain by the Upper Carboniferous. The Lower Permian Kalagang Formation (P_{1k}) consists of gray basalt interbedded with tuffite, thin sandstone and mudstone (Fig. 3). The Carboniferous strata contain more volcanic–sedimentary rocks than those outcropping in the field and show significant southward thinning. This Paleozoic stratigraphic succession suggests that the Tacheng region might have been a remnant ocean basin in Devonian–Carboniferous. In the Late Carboniferous, its rising amplitude was enlarged owing to external compression and, thus, its top denudation and weathering residues were formed. The Kalagang Formation (P_{1k}) was undergoing sedimentation in the Early Permian period, whereas the uplifted areas were apparently denuding because the overlying deposits are visible in the central segment of the Tacheng Basin (profile AA', Fig. 2b). The Tacheng Basin was then covered by the Mesozoic and Cenozoic formations. The seismic data used in this study comprise two industry seismic surveys of high-resolution 2D seismic profiles acquired in 2008. The strata in the Cenozoic and Mesozoic, Permian and the upper part of Carboniferous formations have produced continuous reflection events and clear faults and unconformities, which reflect almost horizontal beds deposited in a relatively stable sedimentary environment. The middle–lower Carboniferous formations, in contrast, are poorly reflective with poor continuity and medium–weak reflection intensities. However, the faults are clearly distinguished and unconformity-bounded and better reflect the severe deformation of this period.

To better constrain on the closure process and time of the remnant ocean, we selected ten Carboniferous volcanic samples from the Well Tacan-1 to study their petrogenetic and tectonic setting characteristics and a tuff for zircon U–Pb dating. Ten basalt and andesite samples were obtained from four different depths (respectively, 952–960 m, 1095–1097 m, 1428–1433 m and 1548–1550 m) (Fig. 3). These samples have high resistivities, medium natural potentials and medium–low natural gamma rays in the logging curve. The rocks are gray or dark gray and massive (Fig. 3). The samples are divided into basaltic andesites and basalt depending on their characteristics under the microscope (Fig. 3). The basaltic andesites consist of phenocrysts of plagioclase, augite, magnetite, hornblende, minor biotite and microcrystals

of plagioclase and augite in a fine-grained groundmass containing several zircon grains. The basalts, which have undergone weak chloritization, contain altered phenocrysts of plagioclase, augite and hornblende in a cryptocrystalline–glassy groundmass that contains magnetite grains (Fig. 3). The groundmass and phenocrysts in the basalts and basaltic andesites have similar characteristics, suggesting that they may be the products of coeval magmatic activity. The main components of the tuff underlying the basalts and andesites are ashes and phenocrysts (Fig. 3). The phenocrysts show irregular edges and are mainly composed of worse crystallized leucocratic mineral and minor calcite debris, but this tuff exhibits homogeneous petrography characteristics under the microscope and were most likely the products of single eruption in a certain magmatic event.

4. Methods and analytical procedures

4.1. LA-ICP-MS U–Pb dating

LA-ICP-MS U–Pb and major and trace element analyses were performed at the State Key Laboratory of Continental Dynamics, Northwest University, Xi'an, China. Handpicked zircon grains were embedded in epoxy and polished down to half size and cleaned in an acid bath before analysis. CL imaging was carried out at the School of Earth and Space Sciences, Peking University. Zircon U–Th–Pb measurements were made on 30 lm diameter regions of single grains using an ICP–MS (Agilent 7500a) and an excimer laser-ablation system (193 nm, Geolas 200M, Lambda Physic). Trace element and U–Th–Pb isotopic data were simultaneously acquired on the same spot. The analytical procedures are similar to those reported by Yuan et al. (2007). The isotopic ratios and element concentration of zircons were calculated using GLITTER (ver. 4.0, Macquarie University). Concordia ages and diagrams were obtained using Isoplot/Ex (ver. 2.94) (Ludwig, 2003). Common lead was corrected using the LA-ICP-MS common lead correction (ver. 3.15) after Andersen (2002).

4.2. Major and trace element analyses

Major element abundances, except FeO and LOI that were analyzed by wet chemical methods, were analyzed by XRF on fused glass disks using the BCR-2 and GBW07105 reference materials. The relative standard deviations of the XRF analyses are less than 2%. Trace elements and REE contents were determined by ICP–MS (Elan 6100DRC), following the method of Gao et al. (1999). The USGS standards (AGV-1, BCR-1 and BHVO-1) were used for calibration. The lowest analytical limit for trace elements is about 0.1 ppm and the analytical accuracies are better than 5% for Co, Ni, Zn, Ga, Rb, Y, Zr, Nb, Hf, Ta and REE (expect Hf and Lu) and 5–10% for the rest.

4.3. Whole-rock Sr–Nd isotope analysis

Sr–Nd isotopic compositions were analyzed at the Institute of Geology and Geophysics, Chinese Academy of Sciences, using a multi-collector VG 354 mass spectrometer in static mode. Approximately 100–150 mg of whole-rock powder was decomposed in a mixture of HF–HClO₄ in screw-top Teflon beakers, and Rb, Sr, Sm and Nd were separated by using cation-exchange columns. Rb, Sr, Sm and Nd concentrations were determined by isotope dilution, using a mixed ⁸⁷Rb–⁸⁴Sr–¹⁴⁹Sm–¹⁵⁰Nd spike solution. Procedural blanks were <200 pg for Sr and <50 pg for Nd. ¹⁴³Nd/¹⁴⁴Nd was normalized to ¹⁴⁶Nd/¹⁴⁴Nd = 0.7219 and ⁸⁷Sr/⁸⁶Sr was normalized to ⁸⁶Sr/⁸⁸Sr = 0.1194. The detailed analytical procedures are described in F.K. Chen et al. (2001). During the course of this study, standards NBS 607 and BCR-1 gave ⁸⁷Sr/⁸⁶Sr of 1.20032 ± 28 (2r) and ¹⁴³Nd/¹⁴⁴Nd of 0.512626 ± 9 (2r), respectively. The analytical precision is ~1% for ⁸⁷Rb/⁸⁶Sr and 0.5% for ¹⁴⁷Sm/¹⁴⁴Nd. The depleted mantle Nd model ages (T_{DM}) were calculated using the present-day depleted mantle ¹⁴³Nd/¹⁴⁴Nd and ¹⁴⁷Sm/¹⁴⁴Nd values of 0.513151 and 0.21357, respectively, and the age of the rock formation.

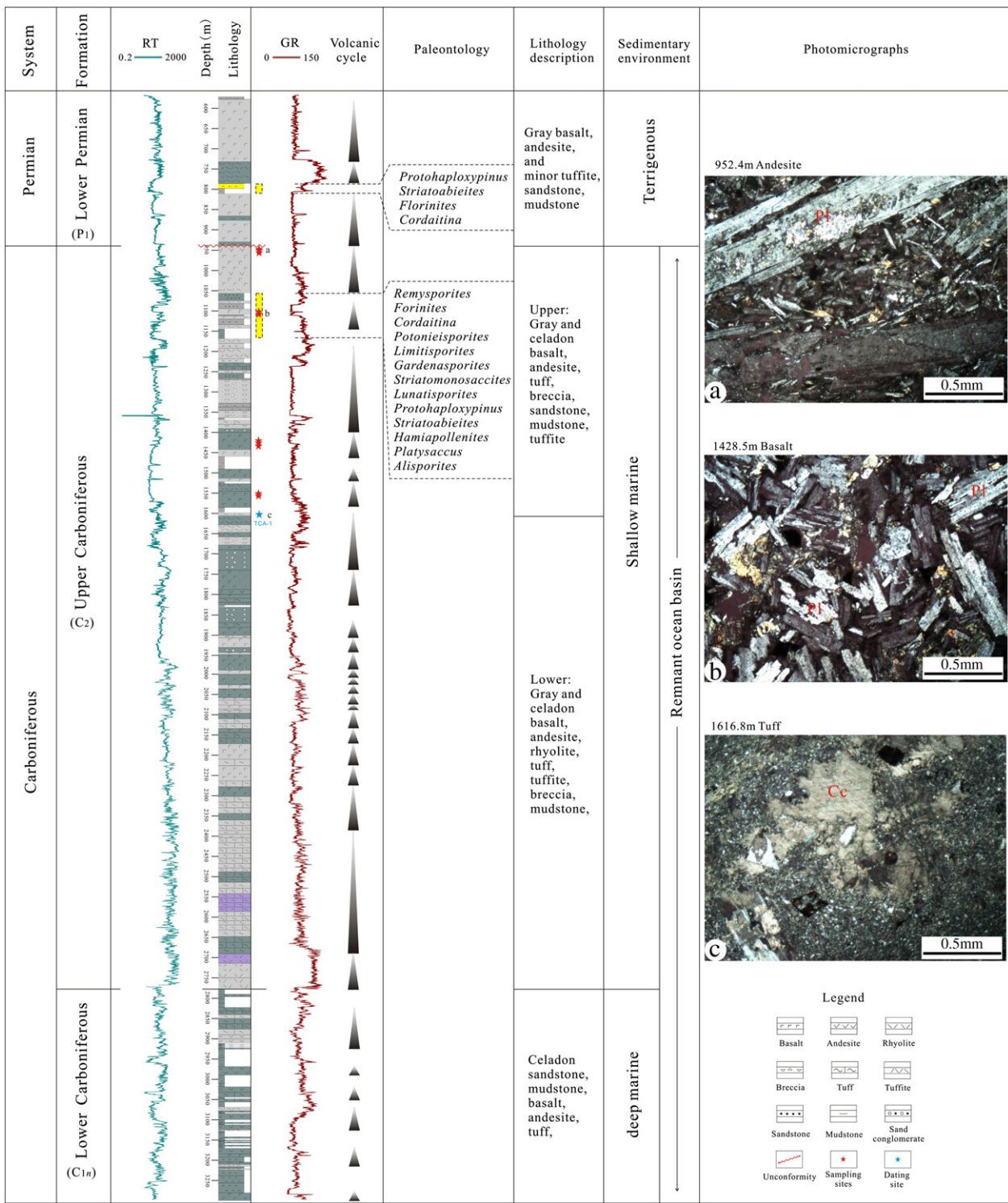


Fig. 3. Comprehensive stratigraphic column of Well Tacan-1 for the generalized log (after Xinjiang Oilfield Company), lithology, volcanic cycle, paleontology, and photomicrographs and the sampling sites of the Carboniferous and Permian strata from the well. The pictures (including a, b, and c) are magnified by 10 × 10 under crossed polars (cp). Pl—plagioclase; Cc—calcite; RT—true formation resistivity; GR—gamma-ray log.

5. Analytical results

5.1. LA-ICP-MS zircon U-Pb dating results

The zircon U-Pb data are summarized in Table 1 and presented in concordia diagrams in Fig. 5a. Thirty-five zircons, analyzed by LA-ICP-MS, were from the tuff (TCA-1) underlying the basalts and andesites. The CL images (Fig. 4) show that most zircon grains are colorless,

transparent to semi-transparent, euhedral to slightly elongate with length between 80 and 100 µm and unclear oscillatory zoning, typical of extrusive rock zircons with length/width ratios of 1.5–2.5. A few zircons contain dark enclaves, others are rounded with sector zoning and several of them contain tiny, relict cores.

Thirty-five zircons from the tuff sample (TCA-1) were analyzed using the LA-ICP-MS U-Pb dating method (Table 1). The results show that all of the analyzed spots fitted along a curve in the U-Pb diagram

(Fig. 5a). The $^{206}\text{Pb}/^{238}\text{U}$ ages ranged from 306 ± 4 Ma to 1763 ± 11 Ma (Fig. 5a) and could be clearly divided into two groups. The younger age group contains 34 analysis spots and $^{206}\text{Pb}/^{238}\text{U}$ ages between 306 ± 4 Ma and 324 ± 11 Ma. These zircons are spread around a $^{206}\text{Pb}/^{238}\text{U}$ age of 315.3 ± 1.6 Ma (Fig. 5b), indicating a Late Carboniferous age. More importantly, all the obtained trace element components and age results from these zircons having different appearances and structure characteristics are both consistent in their error range. In addition, the zircon grains have high and variable U (35.2–290.6 ppm), Th (20.2–313.4 ppm) and Th/U ratios (0.4–1.5 with an average of 0.8) (Table 1), indicating that all the analyzed zircons are of magmatic origin. Based on the results described above, we believe that the age of this suite of tuffs reveals the age of the main magmatic stage in the Tacheng area and provides a lower limit age for the basalts and andesites of Well Tacan-1. In summary, the tuff formed in the Early Carboniferous (315.3 ± 1.6 Ma), indicating that these basalts and andesites formed no earlier than 315 Ma. One zircon has a $^{207}\text{Pb}/^{206}\text{Pb}$ age of 1844 ± 26 Ma or a $^{206}\text{Pb}/^{238}\text{U}$ age of 1763 ± 11 Ma, which may be captured from wall rocks (e.g. sedimentary rocks) during the magma ascent.

5.2. Major and trace elements

Ten samples were analyzed for major and trace elements and the dataset is presented in Table 2. Data sources for the northern Xinjiang adakitic rock (Zhang et al., 2004; Xiong et al., 2005; Zhang et al., 2006; Wang et al., 2007; Mao et al., 2012) and Nb-enriched basalts and basaltic andesites (Zhang et al., 2003, 2004; Wang et al., 2007; Niu et al., 2009; Mao et al., 2012) are also plotted in geochemical diagrams (Fig. 6). For

convenience and detailed discussions, we divide the dataset into four groups, based on the depth in the Well Tacan-1 from where the samples were retrieved. The loss on ignition for the samples in this study ranges from 2.69% (K24-8) to 4.26% (K24-11) except for a sample with a high value of 6.08% (K24-13), suggesting that these samples may be affected by low-temperature alteration, which affected the mobile elements (e.g. K, Na, Rb) (Pearce and Cann, 1973; Winchester and Floyd, 1977).

5.2.1. Magnesian andesites

The andesites have a relatively low, but restricted, range of SiO_2 (54.56–57.29%) and TiO_2 (0.82–0.90%). In the $\text{SiO}_2-(\text{Na}_2\text{O} + \text{K}_2\text{O})$ diagram shown in Fig. 6a, the andesites appear in the basaltic trachyandesite, basaltic andesite and trachyandesite fields. Commonly, they have relatively high MgO (3.61–4.73%, $\text{Mg\#} = 0.53$ –0.59) and low Al_2O_3 (15.38–17.15%) and CaO (3.15–8.02%). Interestingly, the samples have similar Na_2O (3.30–4.77%), K_2O (1.81–2.65%) and CaO (3.15–8.02%) with the magnesian andesites in the western Aleutian Komandorsky region (Yogodzinski et al., 1994, 1995) (Fig. 6c). The content of these major elements compositionally resembles that of typical calc-alkaline high-K rocks (Fig. 6b). Moreover, the samples have adakite-like $(\text{La/Yb})_N$ and Sr/Y ratios, low Y and Yb concentrations (18.02–18.40 and 1.58–1.65 ppm, respectively) (Fig. 7), and negative Nb and Ta anomalies on a primitive mantle-normalized trace element diagram (Fig. 8b and Table 2). Negative Ti and positive Sr anomalies and concave middle and heavy REE patterns are also evident in Fig. 8. These andesites have low Ni (64.4–69.5 ppm) and Cr (87.9–89.1 ppm) concentrations, which makes them comparable to the Alataw adakites in northern Tianshan (Wang et al., 2007). However, the andesites from

Table 1
LA-ICP-MS U–Pb data for zircons from the tuff (TCA-1) underlying the basalts and andesites from Well Tacan-1.

Spot	Th/U	Isotopic contents (ppm)		Isotopic ratios						Apparent age (Ma)					
				$^{207}\text{Pb}/^{206}\text{Pb}$		$^{207}\text{Pb}/^{235}\text{U}$		$^{206}\text{Pb}/^{238}\text{U}$		$^{207}\text{Pb}/^{206}\text{Pb}$		$^{207}\text{Pb}/^{235}\text{U}$		$^{206}\text{Pb}/^{238}\text{U}$	
		^{232}Th	^{238}U	1 s	1 s	1 s	1 s	Age	1 s	Age	1 s	Age	1 s	Age	1 s
1.1	0.5	36.3	72.9	0.0557	0.0031	0.3731	0.0203	0.0486	0.0007	441	121	322	15	306	4
2.1	0.7	66.1	91.8	0.0699	0.0046	0.4755	0.0304	0.0493	0.0009	926	130	395	21	310	5
3.1	0.9	48.8	56.0	0.0607	0.0038	0.4119	0.0253	0.0493	0.0008	627	131	350	18	310	5
4.1	0.6	20.2	35.2	0.0599	0.0049	0.4111	0.0327	0.0498	0.0010	601	167	350	24	313	6
5.1	1.5	271.9	181.2	0.0568	0.0019	0.3856	0.0124	0.0493	0.0005	482	74	331	9	310	3
6.1	0.7	64.5	96.1	0.0595	0.0041	0.4117	0.0278	0.0502	0.0009	585	144	350	20	316	5
7.1	0.7	78.2	110.3	0.0530	0.0028	0.3675	0.0187	0.0503	0.0007	330	115	318	14	316	4
8.1	0.7	46.1	62.5	0.0603	0.0042	0.4119	0.0278	0.0495	0.0009	615	144	350	20	312	5
9.1	0.7	45.8	62.7	0.0553	0.0035	0.3794	0.0234	0.0498	0.0008	425	136	327	17	313	5
10.1	0.8	118.9	153.3	0.0624	0.0025	0.4279	0.0164	0.0497	0.0006	688	83	362	12	313	3
11.1	0.6	31.5	56.4	0.0570	0.0039	0.4000	0.0265	0.0509	0.0008	492	144	342	19	320	5
12.1	0.6	35.6	62.8	0.0615	0.0038	0.4293	0.0257	0.0506	0.0008	657	127	363	18	318	5
13.1	0.9	82.5	91.1	0.0491	0.0035	0.3367	0.0233	0.0498	0.0008	151	158	295	18	313	5
14.1	1.0	102.1	101.5	0.0548	0.0033	0.3884	0.0226	0.0514	0.0008	404	128	333	16	323	5
15.1	0.9	94.7	109.2	0.0517	0.0024	0.3588	0.0163	0.0504	0.0006	271	104	311	12	317	4
16.1	0.6	52.6	82.9	0.0555	0.0036	0.3800	0.0238	0.0497	0.0008	432	138	327	18	312	5
17.1	0.9	299.4	351.2	0.1128	0.0017	4.8905	0.0585	0.3146	0.0022	1844	26	1801	10	1763	11
18.1	0.6	59.7	91.8	0.0572	0.0028	0.3972	0.0188	0.0504	0.0006	498	105	340	14	317	4
19.1	0.7	50.8	77.3	0.0560	0.0030	0.3799	0.0199	0.0492	0.0007	451	116	327	15	310	4
20.1	0.5	59.9	120.0	0.0627	0.0027	0.4369	0.0177	0.0506	0.0006	696	88	368	13	318	4
21.1	0.7	46.6	70.9	0.0529	0.0035	0.3756	0.0244	0.0515	0.0008	326	144	324	18	324	5
22.1	0.6	74.2	119.0	0.0598	0.0030	0.4185	0.0204	0.0508	0.0007	597	106	355	15	319	4
23.1	1.5	309.3	201.2	0.0497	0.0029	0.3360	0.0192	0.0490	0.0006	183	131	294	15	308	4
24.1	0.9	238.8	258.0	0.0538	0.0018	0.3763	0.0117	0.0507	0.0005	363	72	324	9	319	3
25.1	0.6	70.0	120.8	0.0676	0.0032	0.4627	0.0212	0.0497	0.0007	855	96	386	15	313	4
26.1	0.7	197.7	277.1	0.0576	0.0015	0.4015	0.0099	0.0505	0.0004	516	58	343	7	318	2
27.1	0.6	58.6	101.4	0.0539	0.0029	0.3709	0.0190	0.0499	0.0007	368	115	320	14	314	4
28.1	0.7	211.4	290.6	0.0536	0.0015	0.3808	0.0096	0.0515	0.0004	356	60	328	7	324	2
29.1	0.7	26.5	40.1	0.0596	0.0054	0.4112	0.0365	0.0500	0.0011	590	186	350	26	315	7
30.1	1.4	313.4	216.2	0.0541	0.0021	0.3704	0.0134	0.0496	0.0005	377	83	320	10	312	3
31.1	0.6	36.1	62.0	0.0566	0.0036	0.3999	0.0246	0.0513	0.0008	474	135	342	18	322	5
32.1	0.9	78.9	90.3	0.0565	0.0036	0.3862	0.0239	0.0496	0.0008	473	136	332	17	312	5
33.1	0.6	42.1	71.7	0.0540	0.0033	0.3747	0.0224	0.0504	0.0007	370	132	323	17	317	5
34.1	0.4	25.4	57.6	0.0459	0.0035	0.3176	0.0240	0.0502	0.0008	0	167	280	19	316	5
35.1	0.7	52.9	72.7	0.0575	0.0032	0.3899	0.0208	0.0492	0.0007	511	117	334	15	310	4

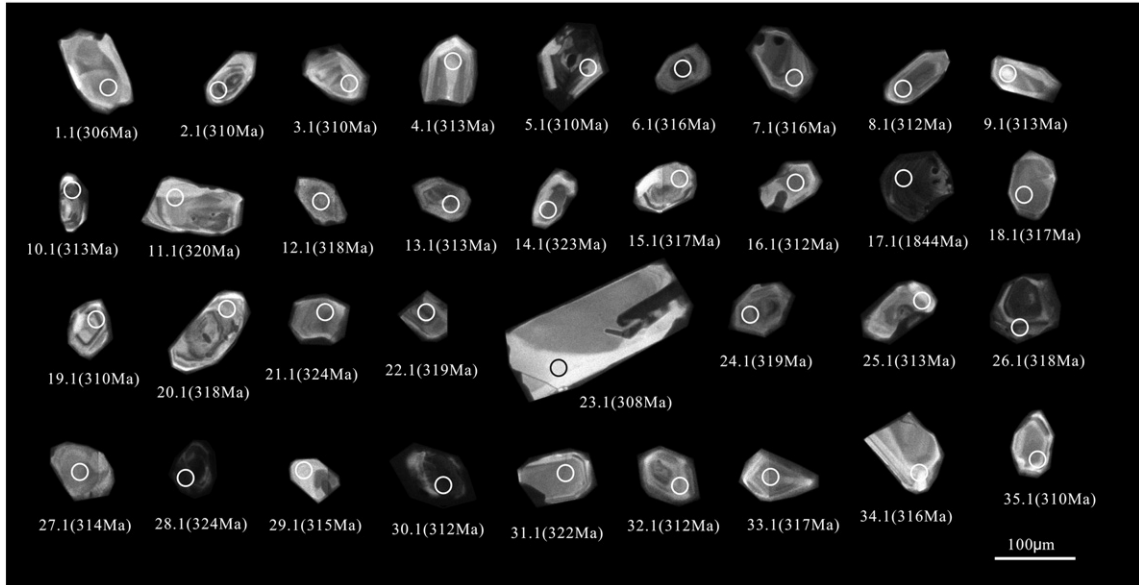


Fig. 4. Representative cathodoluminescence image and LA-ICP-MS U-Pb analyses spots of the zircons from the tuff underlying the basalts and andesites from Well Tacan-1 in the Tacheng Basin (for detailed sample numbers and age of data see Table 1). The circles are zircon LA-ICP-MS U-Pb dating spots.

Well Tacan-1 have higher MgO and Mg# (Table 2), which differentiates them from typical adakitic rocks (Defant and Drummond, 1990) and are more similar to magnesian andesites with some adakitic rock geochemical characteristics.

5.2.2. Basalts

The basalts in Well Tacan-1 are strongly spatially associated with the magnesian andesites. They have low SiO₂ (48.22–51.18%) and fall within the basalt and trachybasalt fields (Fig. 6a). They are sodium-rich (Na₂O/K₂O = 0.31–63; the majority >4) (Fig. 6c) and characterized by relatively higher TiO₂ (1.14–1.50%), P₂O₅ (0.40–0.81%) and Zr (141–181 ppm) contents, and higher (Nb/Th)_{PM} (0.63–1.17), (Nb/La)_{PM} (0.35–0.51) and Nb/U (11.34–29.36) ratios than typical arc basalts (Table 2 and Fig. 9). The total rare-earth-element (\sum REE) content of the basalts from Well Tacan-1 varies between 105 and 153 ppm (Table 2). The chondrite-normalized REE patterns (Fig. 8c) show LREE enrichment ((La/Sm)_N = 2.55–3.24; (La/Yb)_N = 6.83–8.06) and slightly negative or no Eu anomalies (Eu/Eu* = 0.91–1.03), which resembles typical OIB (Sun and McDonough, 1989). The HREE are less

fractionated as revealed by the low ratios of (Gd/Yb)_N (1.80–2.19) similar to N-MORB. Furthermore, these basalts have also similar primitive mantle-normalized trace element content to OIB but tend to have lower Nb/U (11.34–29.36) and Ce/Pb (5.45–18.34) than OIB and MORB (Sun and McDonough, 1989). In addition, all the rocks exhibit some enrichment in LILE (Rb, Ba and K), depletion in Nb and Ta and slightly positive or negative Ba, Sr and Ti (Fig. 8b), indicating that their formation may be related to subduction. Compositionally, two rocks (K24-7 and K24-8) have higher Nb concentrations ranging from 13.80 to 13.95 ppm than most basalts of intra-oceanic arcs (Martin et al., 2005) and are almost identical to those of Nb-enriched basalts in China and elsewhere (Defant et al., 1991; Sajona et al., 1996; Aguillón-Robles et al., 2001; Manya et al., 2007; Wang et al., 2007; Mao et al., 2012).

5.3. Sr-Nd isotope compositions

The Sr-Nd isotopic analysis data for the Carboniferous andesites and basalts from Well Tacan-1 are given in Table 3. Initial ⁸⁷Sr/⁸⁶Sr and

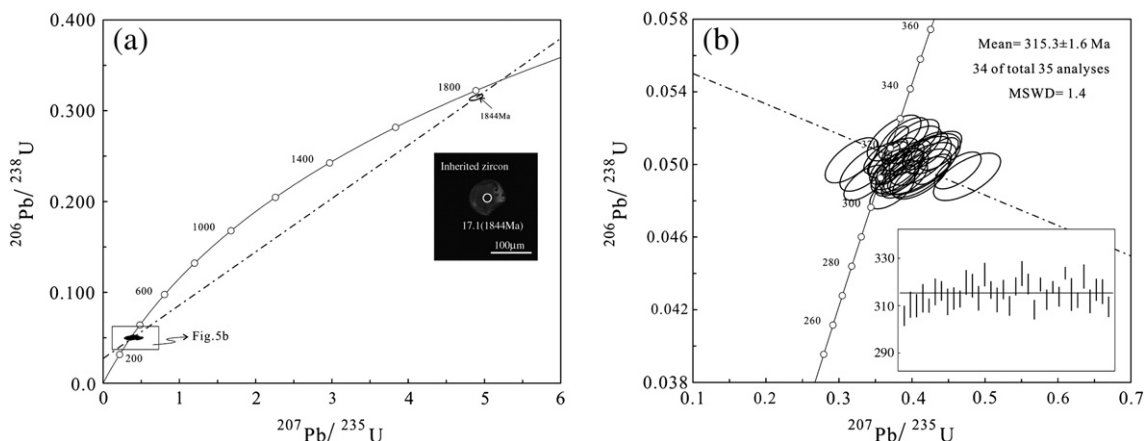


Fig. 5. Zircon LA-ICP-MS U-Pb concordia diagrams of the tuff underlying basalts and andesites from Well Tacan-1 in the Tacheng Basin.

Table 2

Major elements (%) and trace elements (ppm) in the basalts and andesites from Well Tacan-1.

Sample	Andesite			Basalt						
	K24-4	K24-5	K24-6	K24-7	K24-8	K24-9	K24-10	K24-11	K24-12	K24-13
SiO ₂	57.29	55.44	54.56	48.97	51.18	49.43	49.94	48.22	50.54	50.93
TiO ₂	0.88	0.90	0.82	1.49	1.50	1.35	1.41	1.42	1.46	1.14
Al ₂ O ₃	15.38	15.80	17.15	17.03	17.04	16.90	16.38	17.56	17.81	15.26
TFe ₂ O ₃	6.84	7.33	7.02	9.01	9.01	9.20	9.54	9.38	7.55	9.56
MnO	0.10	0.10	0.12	0.12	0.18	0.23	0.22	0.21	0.12	0.12
MgO	4.56	4.73	3.61	5.20	4.20	4.31	3.34	2.80	4.16	5.98
CaO	3.15	4.98	8.02	9.60	8.59	8.76	8.89	10.36	8.70	4.85
Na ₂ O	4.77	4.11	3.30	3.07	3.25	4.62	5.07	4.48	3.95	1.27
K ₂ O	2.65	2.19	1.81	0.85	1.33	0.24	0.08	0.08	0.85	4.12
P ₂ O ₅	0.32	0.32	0.31	0.71	0.72	0.61	0.75	0.81	0.71	0.40
LOI	3.59	3.74	2.89	3.47	2.69	4.00	4.09	4.26	4.11	6.08
TOTAL	99.53	99.64	99.61	99.52	99.69	99.65	99.71	99.58	99.96	99.71
K ₂ O + Na ₂ O	7.42	6.30	5.11	3.92	4.58	4.86	5.15	4.56	4.80	5.39
Na ₂ O/K ₂ O	1.80	1.88	1.82	3.61	2.44	19.25	63.38	56.00	4.65	0.31
Mg#	59	59	53	56	51	51	44	40	55	58
Li	6.85	8.21	7.24	8.20	10.31	21.07	10.32	14.17	8.73	20.07
Sc	20.01	18.49	20.09	20.13	24.25	22.35	23.55	25.20	24.92	19.03
V	164	178	183	213	233	226	250	271	234	183
Cr	87.86	89.14	88.96	148	142	108	105	104	110	84.66
Co	24.04	25.62	22.54	27.23	30.31	32.06	28.67	35.95	28.91	34.05
Ni	66.63	69.49	64.37	74.32	80.77	72.69	63.96	69.55	67.26	67.45
Cu	101	105	84.0	107	107	117	116	115	128	100
Zn	71.97	75.72	72.09	87.32	97.58	89.91	94.32	92.17	101	68.17
Ga	13.87	15.97	19.16	19.57	20.41	18.83	22.67	23.28	20.24	17.05
Rb	43.18	37.19	34.67	5.04	17.29	3.95	2.12	2.40	9.78	55.32
Sr	663	718	803	1032	968	363	268	301	956	590
Y	18.40	18.29	18.02	23.97	25.25	24.96	27.09	27.25	28.62	21.23
Zr	144	144	139	158	160	164	173	181	180	141
Nb	7.13	7.12	6.82	13.80	13.95	9.01	9.35	9.87	9.75	8.10
Cs	0.08	0.13	0.21	0.10	0.18	0.18	0.08	0.12	0.39	1.13
Ba	1306	850	629	557	543	57.3	37.7	47.4	374	713
La	19.50	20.36	21.64	25.92	26.77	24.34	25.83	26.01	27.13	21.44
Ce	41.48	42.21	42.25	55.44	56.76	51.95	55.16	55.31	58.19	45.71
Pr	5.03	5.13	5.02	7.05	7.30	6.61	7.00	6.97	7.44	5.80
Nd	21.27	21.52	21.05	30.93	31.80	28.63	30.49	30.25	32.50	25.27
Sm	4.31	4.32	4.21	6.28	6.44	5.93	6.30	6.22	6.70	5.18
Eu	1.30	1.29	1.32	1.99	2.00	1.77	1.85	1.89	1.94	1.46
Gd	3.90	3.90	3.77	5.54	5.68	5.38	5.67	5.73	6.06	4.62
Tb	0.56	0.56	0.54	0.79	0.81	0.78	0.81	0.83	0.87	0.66
Dy	3.21	3.23	3.18	4.46	4.54	4.42	4.73	4.86	5.03	3.78
Ho	0.64	0.63	0.63	0.86	0.88	0.87	0.93	0.95	0.99	0.73
Er	1.78	1.78	1.72	2.33	2.36	2.40	2.56	2.68	2.73	1.99
Tm	0.26	0.26	0.25	0.34	0.34	0.36	0.38	0.41	0.40	0.29
Yb	1.65	1.62	1.58	2.08	2.10	2.17	2.37	2.57	2.52	1.79
Lu	0.24	0.25	0.24	0.31	0.31	0.33	0.35	0.39	0.37	0.27
Hf	3.22	3.22	3.10	3.39	3.41	3.50	3.65	3.81	3.77	3.13
Ta	0.42	0.42	0.40	0.71	0.72	0.49	0.50	0.52	0.53	0.44
Pb	4.80	6.77	7.58	6.51	6.98	6.67	3.01	4.97	6.79	8.39
Th	2.96	2.93	2.83	1.41	1.56	1.66	1.76	1.82	1.82	1.43
U	0.83	0.83	0.79	0.47	0.48	0.51	0.60	0.87	0.53	0.41
Σ REE	25.78	27.70	27.92	31.18	32.17	31.31	29.17	32.29	34.37	29.39
(La/Yb) _N	8.00	8.47	9.28	8.43	8.60	7.58	7.38	6.83	7.26	8.08
(La/Sm) _N	2.85	2.96	3.24	2.60	2.62	2.58	2.58	2.63	2.55	2.61
(Gd/Yb) _N	1.92	1.95	1.94	2.16	2.19	2.01	1.94	1.80	1.95	2.09
δEu	0.97	0.96	1.01	1.03	1.01	0.96	0.94	0.97	0.93	0.91
Nb/Ta	16.88	16.91	16.96	19.53	19.46	18.40	18.75	19.04	18.43	18.53
Zr/Hf	44.87	44.80	44.87	46.61	46.94	46.97	47.42	47.54	47.58	45.19
Zr/Y	7.84	7.89	7.72	6.60	6.34	6.59	6.38	6.64	6.28	6.66
Ba/La	66.96	41.77	29.07	21.49	20.28	2.35	1.46	1.82	13.80	33.26
Rittmann	3.85	3.19	2.26	2.57	2.56	3.67	3.82	3.98	3.06	3.66

LOI = Loss on ignition, Mg# = $Mg^{2+}/(Mg^{2+} + Fe^{2+}) \times 100$, Eu/Eu* = $Eu_N/(Sm_N \times Gd_N)^{1/2}$, N = chondrite-normalized data.

$\epsilon_{Nd}(t)$ values were calculated for the U-Pb zircon ages (315.3 Ma) for the underlying tuff in Well Tacan-1. All the volcanic rocks from Well Tacan-1 have similar $^{143}Nd/^{144}Nd$ values (0.512752–0.512843) and a narrow range of initial $^{87}Sr/^{86}Sr$ (0.703765–0.703853), indicating that the Sr-Nd isotopic compositions were not affected by alteration (Table 3). The initial $^{87}Sr/^{86}Sr$ ratios in the andesites and basalts are similar (0.703770–0.703853 and 0.703765–0.703829, respectively), but

some variations between the two lithologies are seen. The andesites have $\epsilon_{Nd}(t)$ values of 5.2–6.3 and depleted mantle Nd model ages (T_{DM}) of 565–656 Ma. In contrast, the basalts have higher $\epsilon_{Nd}(t)$ values, between 5.9 and 6.9, and depleted mantle Nd model ages (T_{DM}) between 514 and 603 Ma, suggesting that they may share a common source, even though all the samples lie on the mantle array in the Sr-Nd isotope diagram (Fig. 10).

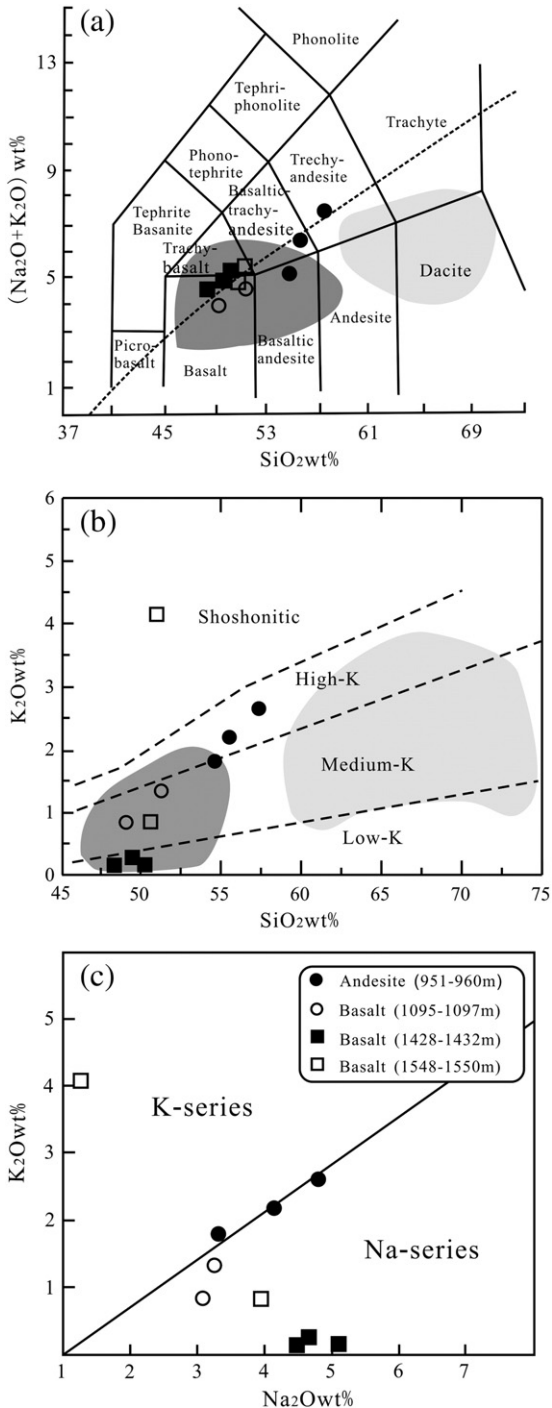


Fig. 6. Geochemical classification diagrams for the volcanic rocks from Well Tacan-1 in the Tacheng Basin. (a) Total alkalis versus silica (TAS) diagram. The dashed boundary line between alkaline and tholeiitic rock types is after Irvine and Baragar (1971); (b) SiO₂-K₂O diagram; (c) Na₂O-K₂O subdivision diagram for the alkaline series. The light and dark shadow fields are reported adakites (Zhang et al., 2004; Xiong et al., 2005; Zhang et al., 2006; Wang et al., 2007; Mao et al., 2012) and Nb-enriched basalts (Zhang et al., 2003, 2004; Wang et al., 2007; Niu et al., 2009; Mao et al., 2012), respectively, in northern Xinjiang in China. Data in panel (a) is after Le Maitre et al., 1989; that in panel (b) is after Peccerillo and Taylor, 1976; and that in panel (c) is after Middlemost, 1975.

6. Discussion

6.1. Alteration and crustal contamination

Basalts from different geodynamic settings have different compositions; as a result, basalts within accretionary belts hold key information

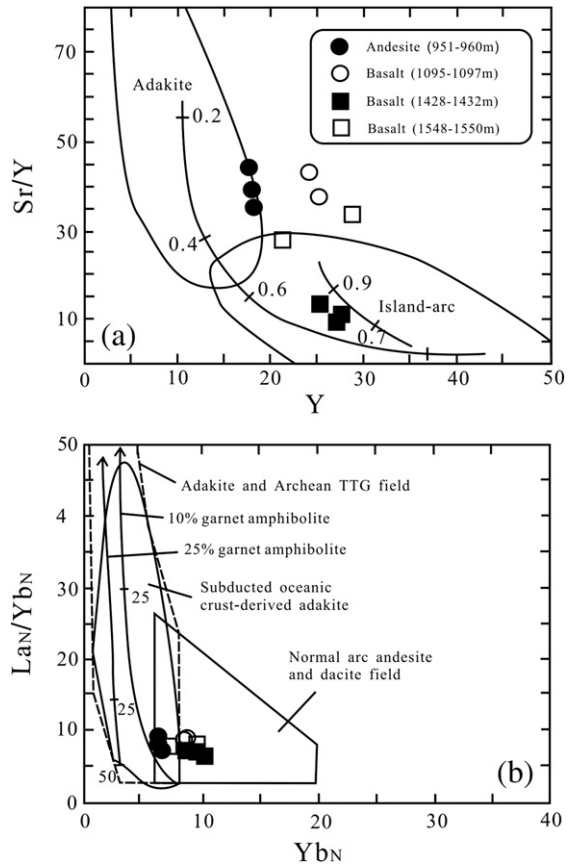


Fig. 7. (a) Sr/Y-Y diagram (Defant and Drummond, 1993) and (b) La_N/Yb_N-Yb_N diagram (Martin, 1999) for andesites and basalts from Well Tacan-1. The fields for subducted oceanic crust-derived adakites are after Wang et al. (2006).

for reconstructing their origin and tectonic evolution. However, after basalt erupts onto the surface or oceanic floor, post-magmatic processes affect its composition. Therefore, the effect of the alteration must be discussed before interpreting basalt geochemistry and reconstructing their geodynamic history.

The REE and primitive mantle-normalized patterns are coherent with a narrow range of absolute abundances and small or no Ce or Eu anomalies (Fig. 8). (Nb/La)_{PM} does not correlate with the CIA (chemical index of alteration), Eu/Eu*, or loss on ignition (Fig. 11). Most samples have LOI < 4.5%. A LOI value of 6.08% in one sample probably reflects the alteration of pyroxene by chlorite. Some Pb mobility is evident in variable troughs relative to Ce and Sr (Fig. 8). REE and HFSE provide strong evidence for low element mobility, as they are considered the least mobile elements (Winchester and Floyd, 1977; Ludden et al., 1982; Condé, 1994). Therefore, we suggest that the geochemical data provide a reliable representation of the original compositions. All the rocks have Mg# values between 0.40 and 0.59, indicating that they were not contaminated by crust. The diagenetic system of the samples is easily identified in the La-La/Sm diagram (Allegre and Minster, 1978). The La/Sm ratio of basalts is nearly constant (4.05–5.14) with, in effect, constant La content (Fig. 12a), suggesting that their petrogenesis is related to fractional crystallization. This is also consistent with the characteristics of the Zr-Zr/Sm diagram (Fig. 12b). The negative Nb anomalies in all the samples seem to reflect some crustal contamination. However, the total trace element content is rather low. The (Nb/La)_{PM} ratios (0.3–0.5) that are greater than 0.25 and do not correlate with the (Th/La)_{PM} ratios (0.44–1.23) and La content (16.7–27.1 ppm) that is higher than 16 ppm, which differs from the typical characteristics of contaminated volcanic rocks from the Vetenry belt (Redman and Keays, 1985; Arndt and Jenner, 1986). Therefore, crustal contamination can be ruled out as a possible mechanism for

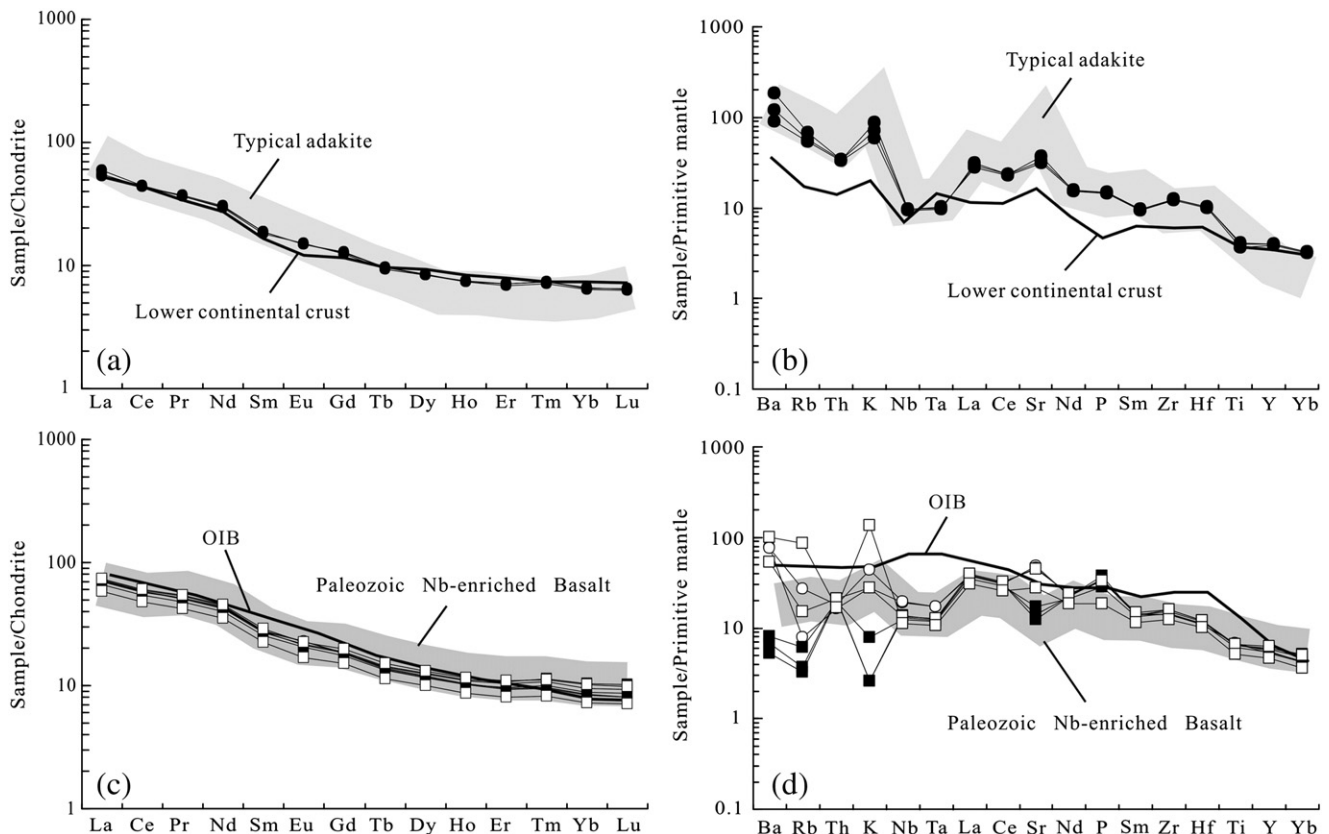


Fig. 8. Distribution of normalized REE and trace elements in volcanic rocks from Well Tacan-1. (a) and (c) Chondrite normalized REE patterns for the samples. The chondritic compositions are after Taylor and McLennan (1985). (b) and (d) Primitive mantle normalized trace element patterns for the samples. The primitive mantle compositions are after Sun and McDonough (1989). The Nb-enriched basalt data for northern Xinjiang are from Zhang et al. (2005), typical adakite data are from Defant et al. (1992). The data for the lower and bulk continental crust are from Rudnick and Gao (2003). OIB normalized data are from Sun and McDonough (1989). The symbols are the same as those in Fig. 6.

causing the observed variations in the radiogenic elements and isotopes and the correlations between elements and isotopes.

6.2. Petrogenesis of the Upper Carboniferous magnesian andesites and basalts

As mentioned above, the Well Tacan-1 magnesian andesites have high Mg# values and low initial $^{87}\text{Sr}/^{86}\text{Sr}$ (0.703770–0.703853) and positive $\varepsilon_{\text{Nd}}(t)$ values (5.2–6.3), suggesting that the samples were derived from partial melting of mantle sources. There are different opinions for the genesis of magnesian andesites. Some researchers consider them partial melts of metasomatized mantle source (Stern and Hanson, 1991; Smithies and Champion, 2000), whereas others favor interaction between mantle and melts from the subducting oceanic slab (Rapp et al., 1999; Smithies et al., 2004, 2007). Most importantly, the magnesian andesites show significant depletion in Y (18.02–18.40 ppm) and HREE (Yb = 1.58–1.65 ppm, <1.8 ppm), high Sr (663–803 ppm) and Ba (629–1305 ppm). The primitive mantle-normalized trace element patterns display positive Sr anomalies and high La/Yb (11.84–13.73) and Sr/Y (36.03–44.55) ratios. In the chondrite-normalized REE diagram (Fig. 8a), all the magnesian andesites display relatively flat patterns with negligible negative or positive Eu anomalies ($\text{Eu/Eu}^* = 0.97$ –1.01). In Sr/Y-Y diagram (Fig. 7a), all the andesites plot in the adakite field. Furthermore, the $(\text{La/Yb})_N$ - Yb_N diagram (Fig. 7b) shows that they have low $(\text{La/Yb})_N$ ratios and mainly plot in the high degree partial melting curve of 10% garnet amphibolite. These geochemical characteristics are similar to the characteristics of adakites formed by subducted young and hot oceanic crust described by Defant and Drummond (1990) and of experimentally determined metabasaltic and eclogitic melts (1–4.0 GPa) (Figs. 8a and 13). However, their MgO

content (3.61–4.73%, >3%; Mg# = 0.53–0.59, >5), is higher than typical adakites (Defant and Drummond, 1990), indicating that the Well Tacan-1 magnesian andesites are not produced by melting of ancient lower continental crust but could have been formed by partial melting of depleted mantle metasomatized by slab melts (Shirey and Harson, 1984; Calmus et al., 2003).

The basalt samples have low SiO₂ (48.22–51.18%) and low Mg# values (40–58) (Table 2), indicating evolved compositions. This is also confirmed by the Zr/Sr-Zr fractional crystallization discrimination diagram (Fig. 12). The similar trace element patterns (Fig. 8c and d) and low initial $^{87}\text{Sr}/^{86}\text{Sr}$ and positive $\varepsilon_{\text{Nd}}(t)$ values suggest that the basalts were derived from depleted mantle source. The high Nb concentrations may result from subduction melts and fluids. The basalts have low Nb/La ratios (0.36–0.53) that are close to those found in typical island arc basalts (<0.5) but different from values found in rift settings (>0.5) (Che et al., 1996; D.L. Chen et al., 2001; Xia et al., 2004a, 2004b; Wang et al., 2006). The enrichment in LILE and LREE suggests hydrous fluid interaction with the overlying mantle wedge, as the mantle is modified by addition of materials from the subducting slab. In addition, the elevated Ba/Nb and low Ba/La ratios (Fig. 14a) suggest significant fluid enrichment at the source. Moreover, the Nb/Zr versus Th/Zr diagram (Fig. 14b) suggests a slab-melt enrichment signature. Thus, we conclude that these basalts may have formed in a subduction-related setting and that both fluids and slab melts were involved in their petrogenesis. Note that two (K24-7, K24-8) of the basalts are similar to calc-alkaline Nb-enriched basalts. Generally, two alternative mantle sources for Nb-enriched basalts have been proposed: (1) an OIB mantle or enriched mantle component in the mantle wedge (Castillo et al., 2002); and (2) a mantle wedge metasomatized by adakites (Defant et al., 1992; Defant and Drummond, 1993; Wyman et al., 2000;

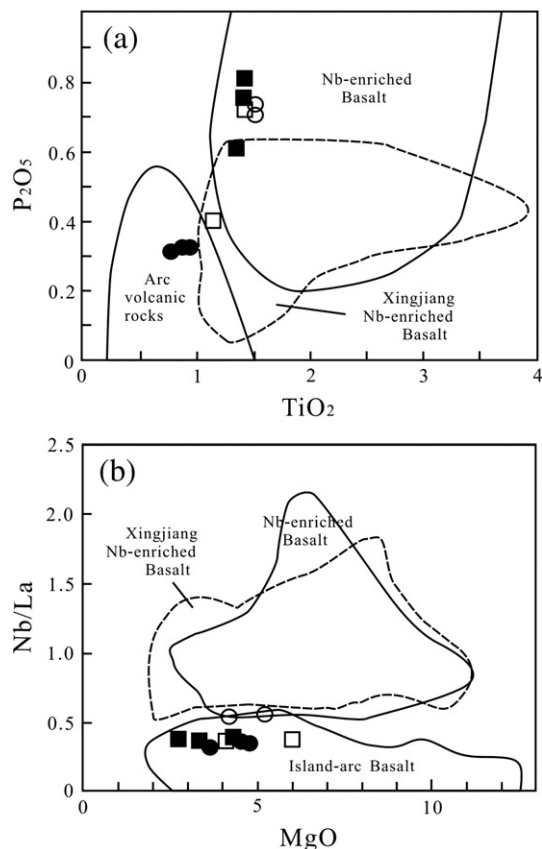


Fig. 9. (a) TiO_2 - P_2O_5 diagram. The arc volcanic rock and Nb-enriched arc basalt fields are from Defant et al. (1992). (b) Nb/La - MgO diagram (Kepezhinskas et al., 1996). The island arc basalt and Nb-enriched basalt fields are from Kepezhinskas et al. (1996). The northern Xinjiang Nb-enriched basalt field is constructed using published data (Zhang et al., 2003, 2004; Wang et al., 2007; Niu et al., 2009; Mao et al., 2012). The symbols are the same as those in Fig. 6.

(Aguillón-Robles et al., 2001; Bourdon et al., 2002; Smithies et al., 2005). The low Nb/U and Ce/Pb ratios in the studied samples show that these Nb-enriched basalts differ from those in OIB ($\text{Nb}/\text{U} = 48$; $\text{Ce}/\text{Pb} = 25$), eliminating the probability of deriving from an OIB mantle. The high Th/Nb ratios (0.10–0.19) are similar to ratios found in EMII-type OIB (Stern et al., 2006) and may be related to the partial melting of sediments above the subducted oceanic crust (Turner et al., 1997). In fact, we consider that the above mentioned mantle source probably played a more important role than source (1) in the petrogenesis of these Nb-enriched basalts because the basalts have a close spatial and temporal association with adakites. Such basalts are thought to derive from the melting of mantle wedge peridotite, which was also previously metasomatized by adakite (Defant et al., 1992; Defant and Drummond, 1993; Sajona et al., 1993, 1996; Kepezhinskas et al., 1996; Aguillón-

Robles et al., 2001; Prouteau et al., 2001; Defant et al., 2002; Wang et al., 2007). In addition, the basalts of Well Tacan-1 have similar initial $^{87}\text{Sr}/^{86}\text{Sr}$ values (0.703765–0.703829) and higher $\varepsilon_{\text{Nd}}(\text{t})$ values (5.9–6.9) compared to magnesian andesites with some adakitic geochemical characteristics but slightly lower than those early Carboniferous volcanics (Fig. 10b). This further supports the notion that their source was previously metasomatized by fluid and slab melts. Several studies have addressed the spatial and temporal association in arcs of normal arc volcanics, magnesian andesites and Nb-enriched basalts (Defant et al., 1991; Yodzinski et al., 1995; Sajona et al., 1996; Yodzinski et al., 2001; Tatsumi and Hanyu, 2003). The association of magnesian andesites and basalts is attributed to (1) adakite liquids from slab melting during subduction of young oceanic crust (Defant et al., 1992; Sajona et al., 1996; Aguillón-Robles et al., 2001; Defant et al., 2002; Wang et al., 2007); (2) the reaction of such liquids with the mantle wedge peridotites, resulting in magnesian magmas; and (3) partial melting of mantle wedge peridotite that is metasomatized by adakitic material and subduction fluids generated Nb-enriched and other basaltic magma, respectively (Kepezhinskas et al., 1996).

6.3. Closure mechanism of the Balkhash–Western Junggar remnant ocean

The Kazakhstan orocline is a horseshoe-shaped belt around the Balkhash–West Junggar remnant ocean, with northern (Chingiz) and southern (North Tianshan) Devonian and late Paleozoic volcanic arcs (Fig. 1b). This orocline played an important role in the closure history of the Balkhash–West Junggar remnant ocean. Large-scale rotations of its northern and southern limbs occurred after Late Devonian because of the compressive stresses exerted by the convergence of the Baltica, Tarim, and Siberia cratons (Zonenshain et al., 1990; Van der Voo, 2004). The rotations have been documented by increasing amounts of paleomagnetic data from both segments of the orocline (Collins et al., 2003; Abrjevitch et al., 2007, 2008; Levashova et al., 2007). To the north, the Saur arc and Irtysh accretionary complex were generated during the final extinction of the Irtysh–Zaysan Ocean by its south-dipping subduction (Fig. 1b) (Buslov et al., 2001, 2004; Windley et al., 2007; Vladimirov et al., 2008; Han et al., 2010), which was confined to the Late Carboniferous (Zhou et al., 2008; Kuibida et al., 2009; Chen et al., 2010), indicating that the interaction between the Kazakhstan orocline and the Siberian craton continued into the Late Carboniferous. To the south, although arc–continent collision was mentioned by Abrjevitch et al. (2008), the northward subduction of the South Tianshan Ocean still took place during the Carboniferous, based on ultrahigh-pressure and high-pressure metamorphism (Gao et al., 1994, 1995, 1998; Gao and Klemd, 2000). Some Late Carboniferous to Permian ages of the ultrahigh-pressure metamorphic rocks in SW Tianshan (Zhang et al., 2007) and the Late Permian radiolarian fossils in the accretionary complex along the South Tianshan (Li et al., 2005) indicate that the subduction likely continued to Permian. Although controversial, the closure of the South Tianshan Ocean has been proposed to be either in the Carboniferous based on Carboniferous peak

Table 3

Whole rock Sr–Nd isotopic compositions of the basalts and andesites from Well Tacan-1.

Sample	Rock	Rb (ppm)	Sr (ppm)	$^{87}\text{Rb}/^{86}\text{Sr}$	$^{87}\text{Sr}/^{86}\text{Sr}$	2σ	$(^{87}\text{Sr}/^{86}\text{Sr})_i$	Sm (ppm)	Nd (ppm)	$^{147}\text{Sm}/^{144}\text{Nd}$	$^{143}\text{Nd}/^{144}\text{Nd}$	2σ	$\varepsilon_{\text{Nd}}(\text{t})$	T_{DM} (Ma)
K24-4	Andesite	43.2	663	0.188401	0.704615	11	0.703770	4.31	21.3	0.122469	0.512752	9	5.2	656
K24-6	Andesite	34.7	803	0.124888	0.704413	9	0.703853	4.21	21.0	0.120952	0.512805	14	6.3	565
K24-7	Basalt	5.04	1032	0.014121	0.703892	9	0.703829	6.28	30.9	0.122693	0.512802	12	6.2	576
K24-8	Basalt	17.3	968	0.051652	0.704044	8	0.703812	6.44	31.8	0.122408	0.512785	12	5.9	603
K24-9	Basalt	3.95	363	0.031442	0.703953	14	0.703812	5.93	28.6	0.125301	0.512841	13	6.8	521
K24-11	Basalt	2.40	301	0.023093	0.703918	11	0.703814	6.22	30.2	0.124267	0.512843	9	6.9	514
K24-12	Basalt	9.78	956	0.029586	0.703920	11	0.703787	6.70	32.5	0.124720	0.512840	11	6.8	521
K24-13	Basalt	55.3	590	0.271108	0.704980	13	0.703765	5.18	25.3	0.123880	0.512829	12	6.7	536

$^{87}\text{Rb}/^{86}\text{Sr}$ and $^{147}\text{Sm}/^{144}\text{Nd}$ ratios calculated using Rb, Sr, Sm and Nd contents, measured by ICP-MS.

$\varepsilon_{\text{Nd}}(\text{t})$ values calculated using present-day $(^{147}\text{Sm}/^{144}\text{Nd})_{\text{CHUR}} = 0.1967$ and $(^{143}\text{Nd}/^{144}\text{Nd})_{\text{CHUR}} = 0.512638$.

T_{DM} values calculated using present-day $(^{147}\text{Sm}/^{144}\text{Nd})_{\text{DM}} = 0.2137$ and $(^{143}\text{Nd}/^{144}\text{Nd})_{\text{DM}} = 0.51315$.

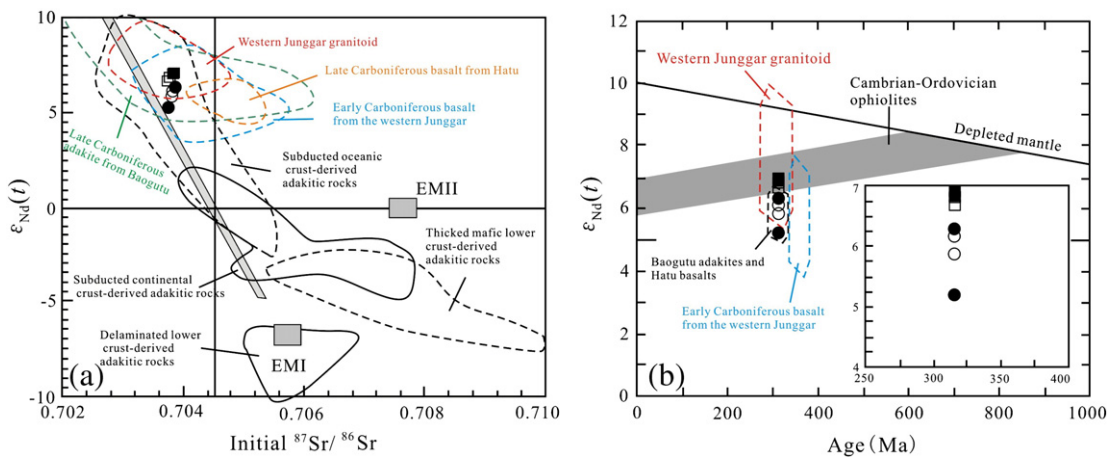


Fig. 10. Plots of $\epsilon_{\text{Nd}}(t)$ values versus initial $^{87}\text{Sr}/^{86}\text{Sr}$ ratios (a) and the age of the volcanic rocks (b) from Well Tacan-1 compared with the western Junggar ophiolites and Carboniferous volcanic rocks in the western Junggar region. Subducted oceanic crust-derived adakites and thickened and delaminated mafic lower crust-derived adakitic rocks are after Wang et al. (2006), Huang et al. (2008) and references therein. Subducted continental crust-derived adakites are after Wang et al. (2008). The Hatu basalts are from Tang et al. (2012b), the Baogutu adakites are from Tang et al. (2010), the Early Carboniferous normal arc-type volcanic rocks are from Geng et al. (2011); and the western Junggar granitoids are from Chen and Arakawa (2005) and Geng et al. (2009). Data for the Cambrian–Ordovician ophiolites are from Zhang and Huang (1992) and the enriched mantle EMI and EMII members (Hart, 1988) are shown for comparison.

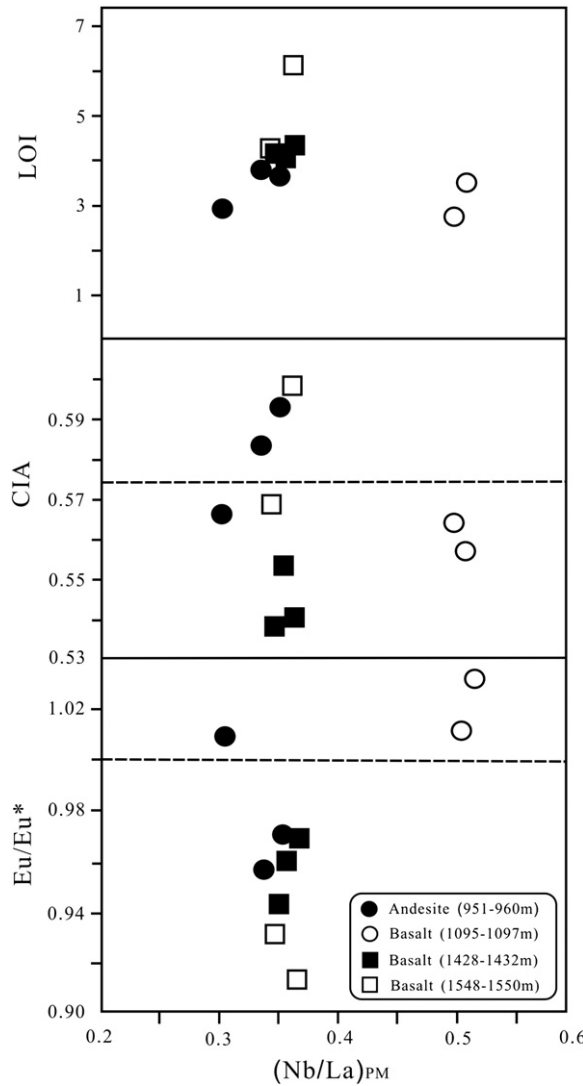


Fig. 11. $(\text{Nb/La})_{\text{PM}}$ versus loss on ignition (LOI), chemical index of alteration (CIA) and Eu/Eu^* (Nesbitt and Young, 1982) for the volcanic rocks, indicating that the Nb–La inter-element ratios do not correlate with alteration and metamorphism. The dashed lines are primitive mantle ratios from Sun and McDonough (1989) ($\text{CIA} = \text{Al}_2\text{O}_3/(\text{CaO} + \text{Na}_2\text{O} + \text{K}_2\text{O} + \text{Al}_2\text{O}_3)$).

metamorphic age of high-pressure rocks (Gao et al., 1994; Han et al., 2010) or even in the Permian based on the facts of Carboniferous to Permian ages of the ultrahigh-pressure metamorphic rocks and the Late Permian radiolarian fossils in the accretionary complex in South Tianshan (Xiao et al., 2013). These facts suggest that external compressive stress, resulting from the motion of the converging Siberia and Tarim cratons, is an important mechanism involved in the Kazakhstan oroclinal bending and the closure of the Carboniferous Balkhash–West Junggar remnant ocean.

As the basin is filled with clastic components generated by the uplift and denudation of the surrounding orogenic belt, a number of volcanic rocks and volcanioclastic rocks also entered the Balkhash–West Junggar remnant ocean basin. This feature requires its own geodynamic mechanism. Carboniferous strata outcropping in western Junggar is mainly dominated by volcanic–sedimentary rocks, such as tuff, tuffaceous sandstone, siltstone and chert, intercalated with mafic and intermediate lavas. Recently, the U–Pb age of tuff from the Carboniferous Tailegula and Baogutu Formations in the southern western Junggar terrane was estimated between 328 and 342 Ma (Wang and Zhu, 2007; An and Zhu, 2009). Furthermore, calc-alkaline rocks with adakitic affinities were described and their formation was attributed to slab melting and

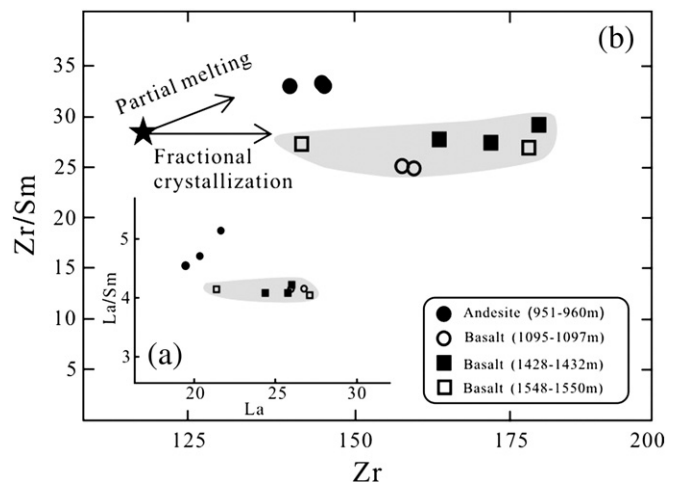


Fig. 12. (a) La–La/Sm diagram and (b) Zr–Zr/Sm diagram for the andesite and basalt samples from Well Tacan-1. Data in panels (a) and (b) are after Allegre and Minster, 1978.

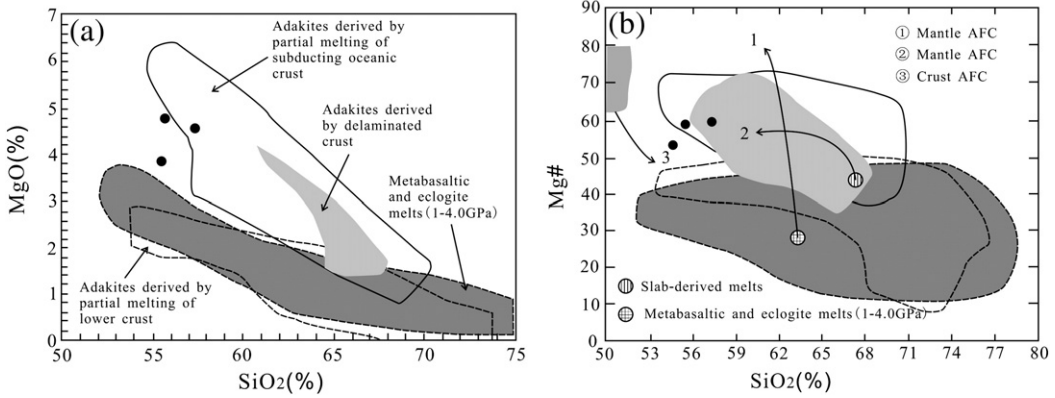


Fig. 13. (a) SiO₂-MgO diagram and (b) SiO₂-Mg# diagram (Peccerillo and Taylor, 1976) for the andesites from Well Tacan-1. The subducting oceanic crust-derived adakite field was constructed using data from Defant and Drummond (1990), Stern and Kilian (1996), Martin (1999), Smithies (2000), and Defant et al. (2002). The eclogitic metabasalt (1–4 GPa) field is from Sen and Dunn (1994), Rapp and Watson (1995) and Springer and Seck (1997). The lower crust-derived adakite field is from Atherton and Petford (1993), Muir et al. (1995), Petford and Atherton (1996) and Smithies (2000). Curves 1 and 3 are from Stern and Kilian (1996) and curve 2 is from Rapp et al. (1999). The symbols are the same as those in Fig. 6.

ridge subduction (Geng et al., 2009; Zhang et al., 2011a). The Late Carboniferous magmatic suites consisting of A-type and I-type plutons may have resulted either from the post-collisional environment (Chen and Arakawa, 2005; Han et al., 2006; Su et al., 2006) or from the subduction-dominated regime (Zhang et al., 2006; Xiao et al., 2009). It is difficult to constrain their formation in the Late Carboniferous tectonic setting because of the lack of complete and accurate successions in the Late Carboniferous stratigraphic data.

Our petrogenesis analysis shows that the Well Tacan-1 basalts and andesites were generated by partial melting of mantle wedge peridotites, which were previously metasomatized by adakites, showing that

hot oceanic crustal subduction and slab melting were important crustal growth mechanisms in the CAOB (Geng et al., 2009; Tang et al., 2009; Yin et al., 2010). The basalts and andesites were confirmed as being Late Carboniferous, indicating that oceanic slab subduction and melting still occurred in the Tacheng area in the Late Carboniferous. On the Y/15-La/10-Nb/8 (Cabanis and Lecolle, 1989) and Ti/100-Zr-Y*3 (Pearce and Mei, 1990) diagrams, all the samples fall into the calc-alkaline basalt field (Fig. 15a, d) and this is supported by the Hf/3-Th-Ta discrimination diagrams (Fig. 15c) (Wood, 1980; Wood et al., 1981). These characteristics, in combination with the compressive structural deformation from the seismic profile mentioned above and regional geology (Xiao et al., 2008; Zhang et al., 2011b), support the conclusion for a subduction-related tectonic setting for the Tacheng area in the Late Carboniferous. Therefore, the andesites and basalts from Well Tacan-1 in the Tacheng Basin suggest that the subduction-related tectonic environment in the Late Carboniferous was an important closure mechanism of the Balkhash-West Junggar remnant ocean. Based on the accumulation of Permian coarse red sandstones and conglomerates in the field (Feng et al., 1989; Allen et al., 1995; Jin and Li, 1999; Buckman and Aitchison, 2004) and the unconformity between Carboniferous and Low Permian in the basin, the continuous subduction in western Junggar probably ended before the Early Permian (Choulet et al., 2012).

6.4. The sedimentary filling and closure process for the Balkhash–Western Junggar remnant ocean

The study of western Junggar accretionary processes requires understanding the relation between the convergent setting and the tectonic-sedimentary evolution of the Balkhash–West Junggar remnant ocean basin. The sedimentary filling and closure history of the Balkhash–West Junggar remnant ocean basin involved contributions from subduction and accretion, recorded in the strata of Well Tacan-1. The Carboniferous strata of Well Tacan-1 at the Southern Depression of the Tacheng Basin record moderate–high magnetic anomalies, similar to the magnetic anomaly characteristics of volcanic rocks on both sides of the Darbut suture zone and the intermediate–basaltic volcanic rocks in the Luliang area in the north of Junggar Basin (L. Zhou et al., 2006). The distribution and lithologic features of these volcanic rocks also match the Carboniferous volcanic rocks that outcrop in southern West Junggar. In the 2D seismic profiles of the Tacheng area, the faults can be clearly distinguished by the seismic reflector wave cut-offs (Fig. 16). The seismic interpretation reveals two groups of faults. The first cuts the Upper Carboniferous and has westward-verging thrust imbricates with growth strata in the eastern area of the Tacheng Basin, whereas the second cuts the Mesozoic to Cenozoic and shows eastward-verging thrust imbricates in the western area of the Tacheng

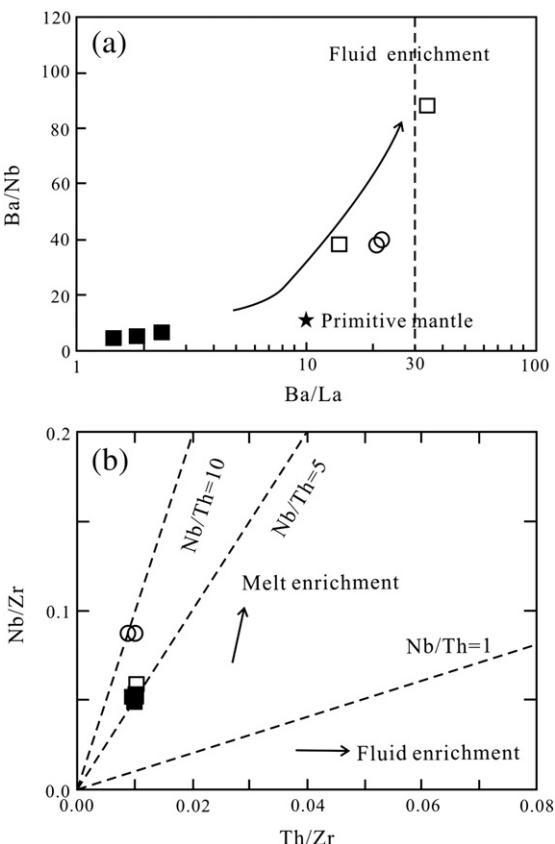


Fig. 14. Plots of (a) Ba/Th-Th and (b) Nb/Zr-Th/Zr diagrams for the andesite and basalt samples from Well Tacan-1. The symbols are the same as those in Fig. 6. Data in panel (b) is after Geng et al., 2011.

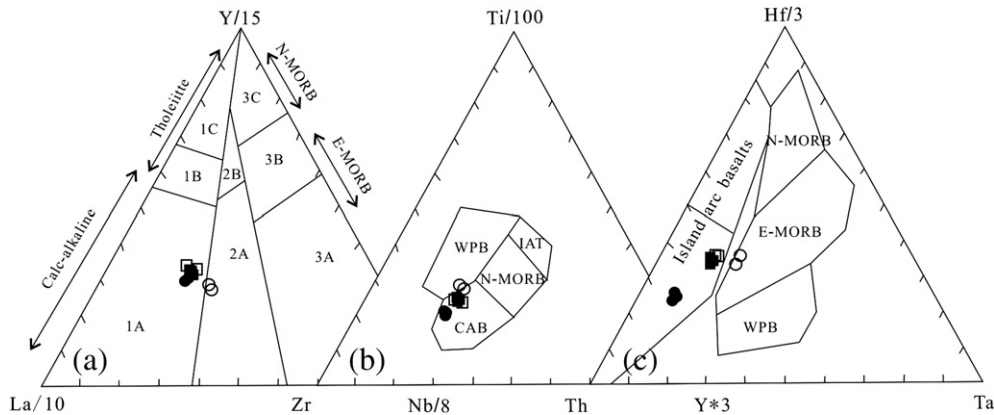


Fig. 15. Tectonic setting discrimination diagram for andesite and basalt samples from Well Tacan-1. (a) Y/15-La/10-Nb/8 diagram for samples; (b) Ti/100-Zr-Y*3 diagram. (c) Hf/3-Th-Ta diagram. 1A—calc-alkaline, 1C—volcanic arc tholeiites and 1B—overlap area between 1A and 1C; 2A—continental basalts, 2B—back-arc basin basalts; 3A—alkali basalts; 3B—enriched MORB; 3C—depleted MORB; WPB—within-plate basalt; IAT—Island tholeiite; CAB—Calc-alkaline basalt. The symbols are the same as those in Fig. 6. Data in panel (a) is after Cabanis and Lecolle, 1989, panel (b) after Pearce and Mei, 1990, and panel (c) after Wood, 1980; Wood et al., 1981.

Basin. These thrust faults dip steeply at shallow depths and gently at greater depths, and the thrust displacement dies out upwards. The geometry characteristics and growth strata suggest that these westward-thrust faults caused Late Carboniferous deformation in the hanging wall layers. In addition, several faults in the central segment of the Tacheng Basin have steep dip angles (80° – 90°), similar to the Darbut strike-slip fault, which developed in response to the strain partitioning during oblique subduction (Choulet et al., 2012).

Considering the strata drilled in Well Tacan-1 (Fig. 3), we divide the Carboniferous–Early Permian strata that filled the Tacheng Basin into two tectonostratigraphic units (Fig. 16), because of the lithological combinations and unconformity between the Carboniferous and Lower Permian. The first one (Carboniferous tectonostratigraphic–T1) includes 29 periods of volcanic activity with tuff and tuffite intercalated with minor mudstone, sandstone and conglomerates. However, the Early and Late Carboniferous exhibit significant differences in the rock associations. The Early Carboniferous strata consist of tuff, sandstone and mudstone with minor andesite and basalt. The regionally distributed sandstone and interbedded mudstone were deposited as turbidites during the early ‘starved’ stages in the basin and the thinness of the marine sedimentary fill attests to the tectonic instability of the basin and the occurrence of re-sedimentation processes (Jin and Li, 1999). There were multiple periods of sedimentary intermission, during which thin gray–black mudstone formed. The abundance of tuff and arc-related lavas in the basin fill indicates that there was volcanism nearby. Furthermore, the early Carboniferous strata preserved within the basin are similar to those on both sides of Darbut, indicating a deep-sea environment (Li and Jin, 1989; Jin and Li, 1999; Guo et al., 2002). Moreover, at the eastern side of the Tacheng Basin, the geochemical characteristics of the 328 Ma Baobei volcanic rocks and some 321 Ma magnesian diorite dikes with high Sr/Y ratio indicate that they formed in an oceanic island arc setting in the Late Carboniferous (Zhu and Feng, 1994; Wang and Sun, 2005; Yin et al., 2010). Nearly all the Late Carboniferous strata consist of basalt, andesite and tuff, except for minor mixed marine and non-marine deposits in the upper parts. The identification of Late Carboniferous magnesian andesites and basalt supports an island arc tectonic setting in the Late Carboniferous. This is compatible with the recent conclusions regarding the NW-directed subduction in western Junggar (Geng et al., 2009; Tang et al., 2009; Yang et al., 2012). The occurrences of the Late Carboniferous adakite, Nb-enriched basalt and charnockites suggest that the western Junggar accretionary complex is formed by north-westward subduction in the Late Carboniferous. Although the north-westward subduction for the western Junggar arc was established in the modern Darbut area (Geng et al., 2009; Liu et al., 2009; Tang et al., 2009), this was a relatively mature island arc

with adakitic magmatism during the Late Carboniferous, whereas intra-oceanic normal subduction still occurred in the Tacheng area. Thus, we suggest that the abundant tuff and interbedded lavas in the Tacheng area were generated from another subduction system and the minor mudstone deposits indicate a shallow sea sedimentary sequence in the Late Carboniferous. The decreasing volcanic activity and the transition from marine to non-marine facies indicate that the remnant ocean basin was shrinking during the Late Carboniferous. The obvious unconformity between Carboniferous and Early Permian was tied from Well Tacan-1 to seismic data. The Early Permian molasses locally overly the western Junggar accretionary complex (Jin and Li, 1999) and are preserved in the northern Paleozoic Saur volcanic arc (Chen et al., 2010). In addition, the Latest Carboniferous–Middle Permian stitching plutons crosscut all of the western Junggar and the adjacent Kazakhstan tectonic units with several mélange belts (e.g. Karamay mélange, Darbut ophiolitic mélange, Barleik mélange and Irtysh–Zaysan ophiolitic mélange). All these data indicate that the closure of the Balkhash–West Junggar remnant ocean most likely occurred in Early Permian and got into intracontinental evolution. The Early Permian strata of Well Tacan-1 only contain three periods of volcanic activity with mainly basalt, andesite, tuffite and terrigenous buff sand conglomerates, sandstone and mudstone, which represent the sedimentary response to the closure of remnant ocean. Moreover, the Early Permian strata become progressively thicker toward the west, suggesting that the Early Permian source was from the N/NW of the basin. This was also controlled by the uplift of the western part of the Tacheng Basin, resulting from an Early Permian NW-oriented thrust fault (Fig. 16). Depth conversion of the seismic profile AA' was performed using the averaged interval velocity for the stratigraphic restoration calculation shown in Fig. 17. A balanced cross-section is a structural cross-section that is consistent with and can be restored to its pre-deformation state (Dahlstrom, 1969; Woodward et al., 1989). During the Carboniferous, the Tacheng region was undergoing EW shortening and the amount of shortening is approximately 3.9 km on the profile AA' (Fig. 17). The Carboniferous strata were shortened by approximately 0.8 km between the Jurassic and the present (Fig. 17). In contrast, the closure of the Balkhash remnant ocean most likely occurred in the Early Carboniferous and earlier than that of the western Junggar remnant ocean, because the Early Carboniferous siliceous rocks that contain Ordovician conodonts in western Junggar are found in the Silurian strata of the Balkhash region (Fig. 18). In addition, the Devonian strata in northern Balkhash and Bakanas–Alakol of East Kazakhstan represent a very thick flysch consisting of interbedded sandstone and siltstone with some limestone. The depositional characteristics are similar to those of the Carboniferous western Junggar remnant ocean. Moreover, non-marine unconformities

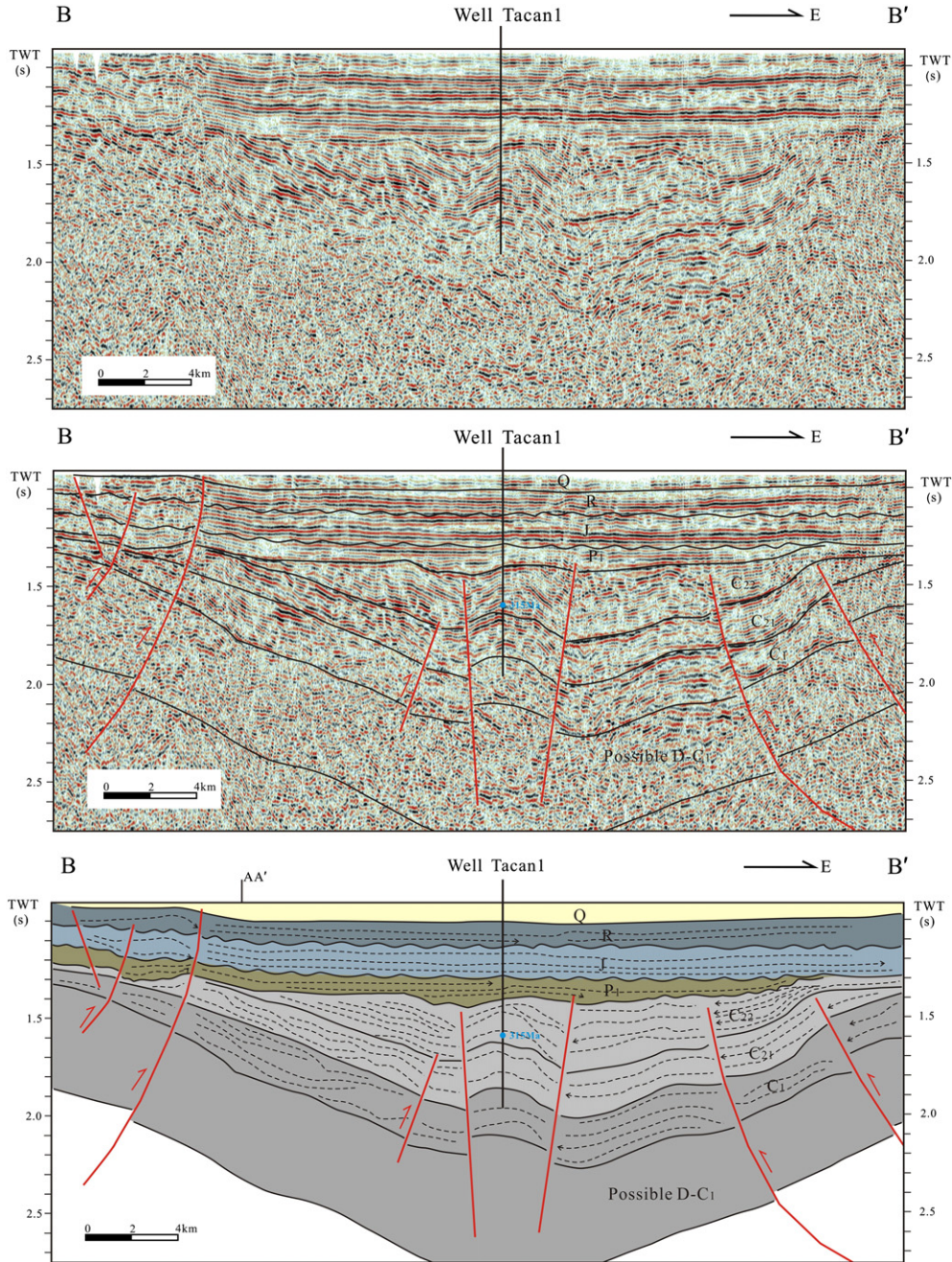


Fig. 16. Seismic profile AA' and its geological interpretation in the Tacheng Basin (the primitive seismic profile was provided by the Xinjiang oilfield company, CNPC).

occurred from Devonian to Carboniferous in the Kazakhstan area, whereas they took place in Late Carboniferous to Early Permian in the western Junggar region. This is further confirmed by the similar rock associations between the Upper Carboniferous in the Tacheng area and the Lower Carboniferous in the Balkhash area (Fig. 18). These features indicate that the Balkhash–West Junggar remnant ocean experienced a scissors-type closure from Balkhash to western Junggar since the Early Carboniferous. However, the existence of dolomite in the boreholes suggests that the western margin of the Junggar Basin was a shallow sea sedimentary environment in the Late Carboniferous.

Based on the above discussion regarding the tectonic setting and tectonic-sedimentary evolution, a fill model for the Balkhash–West Junggar remnant ocean basin was proposed since Carboniferous in western Junggar (Fig. 19). During the Early Carboniferous (Fig. 19a),

the western Junggar region was in a subduction-related tectonic setting and some deep-sea facies volcano-originated sediments filled in the remnant ocean basin. With the shrinking of the ocean basin, strong thrusting at the southeast of the ocean basin resulted in uplifts at the basin boundary and the shallow-sea facies volcanoclastic rocks with minor non-marine sediments from the southeast of the ocean filled the basin (Fig. 19b). By the Early Permian, the sedimentary environment had changed to terrigenous facies with detritus from the north of the basin (Fig. 19c). At the eastern margin of the remnant ocean basin, the Early Permian strata overlap the Carboniferous strata, indicating the end of the filling of the remnant ocean basin. At the western end of profile AA', the Carboniferous strata are thinner toward the west, unlike the Early Permian and Meso-Cenozoic. This may reflect multi-stage thrusting or re-activation of previous thrust faults. The amalgamation of island

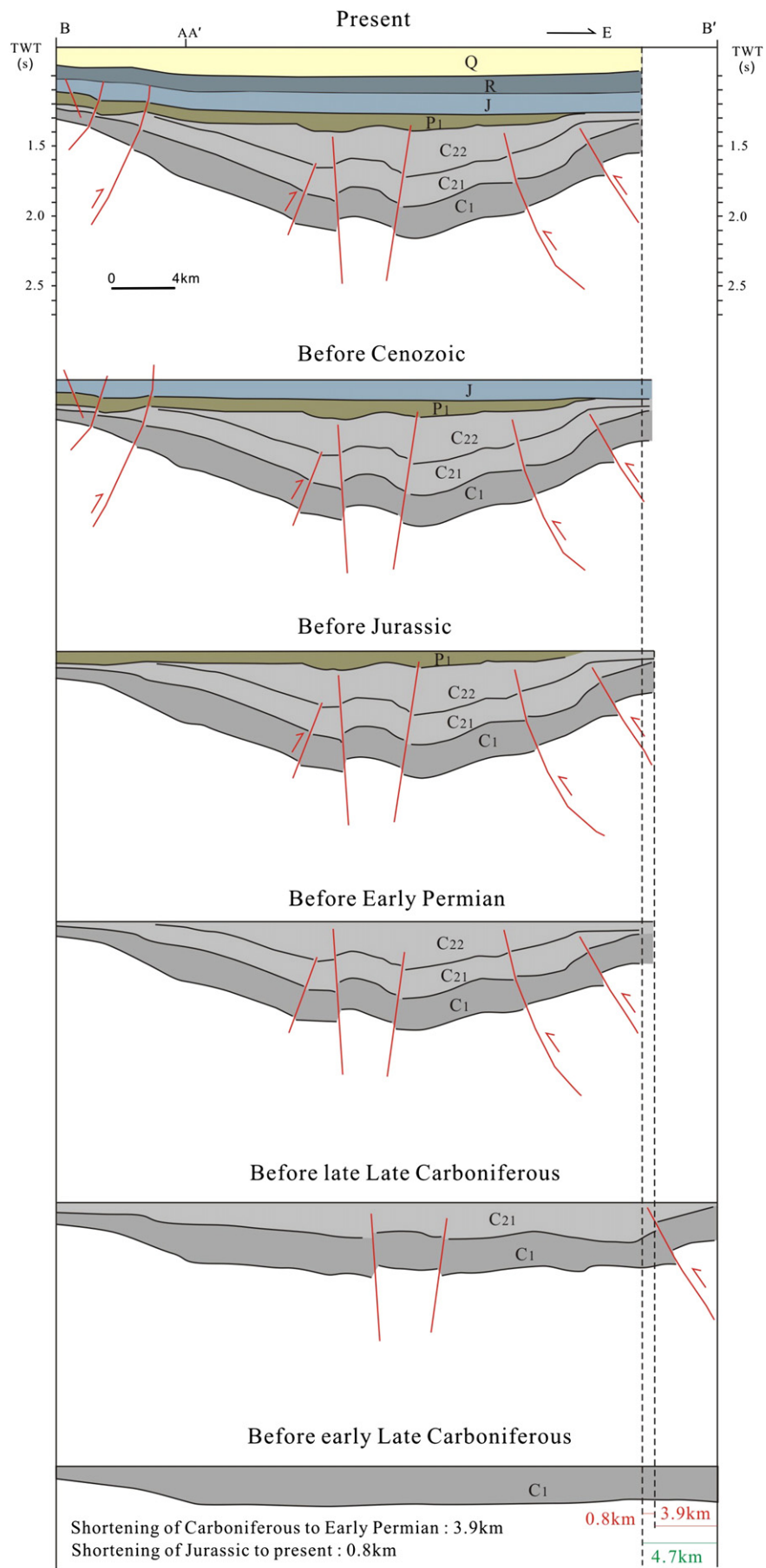


Fig. 17. Balanced cross section and structural-stratigraphic restoration of seismic profile AA' since the Early Carboniferous (the position of seismic profile AA' is shown in Fig. 1c).

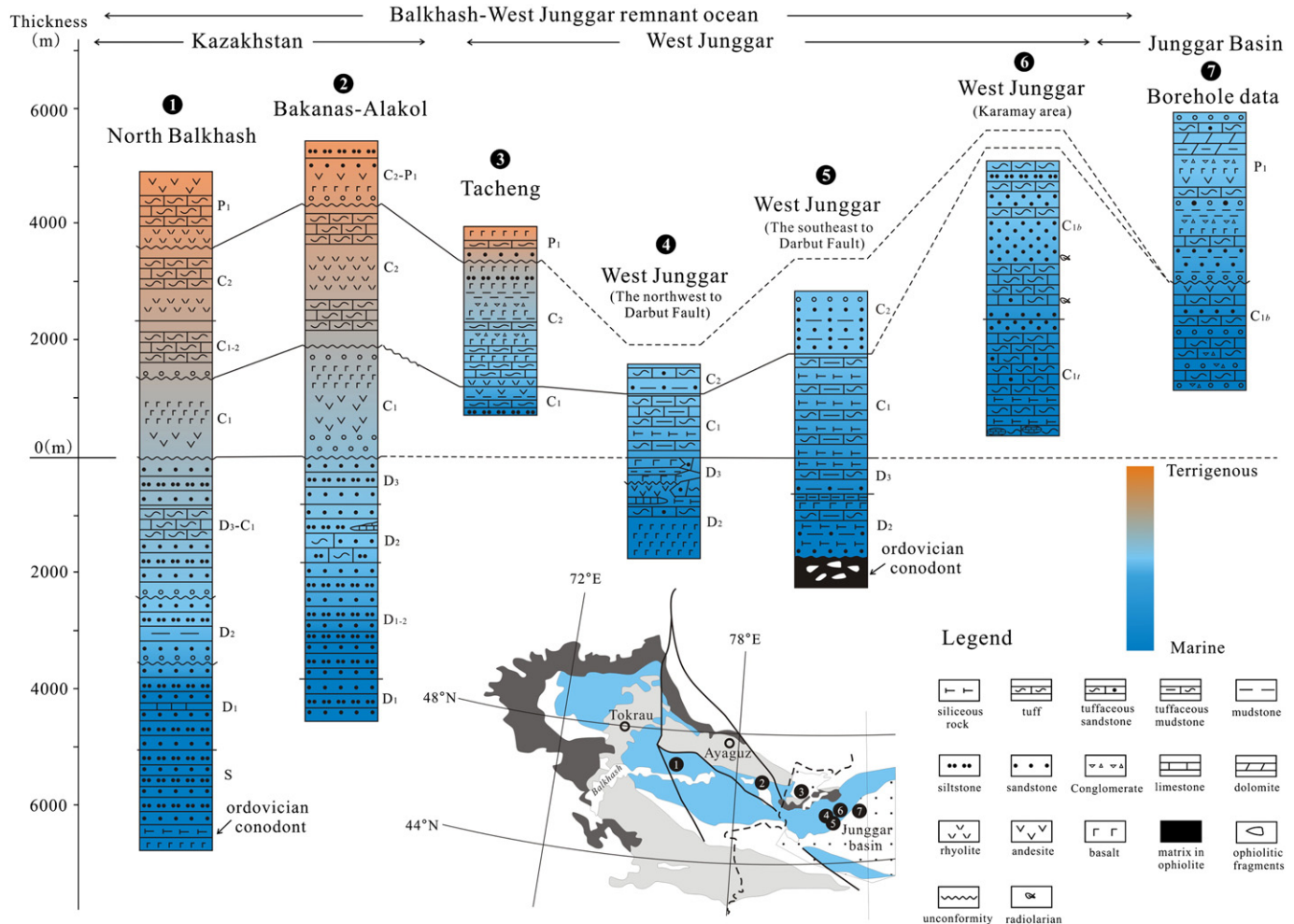


Fig. 18. Stratigraphic columns in the West Junggar and Balkhash region. The column positions are shown in Fig. 1b and this figure. Modified after Samygin et al., 1997; Zhao and He, 2013.

arcs and accretionary complexes, combined with sedimentary filling, led to the closure of the Balkhash–West Junggar remnant ocean and finally formed the basement of the Meso-Cenozoic Tacheng Basin.

7. Conclusions

Using geochronological and whole-rock geochemical data, tectonostratigraphic unit analysis and a range of technologies and methods on volcanic rocks from Well Tacan-1 in the Tacheng Basin, we concluded the following:

- (1) Zircon U–Pb analysis of the underlying tuff suggests that the andesite and basalt from Well Tacan-1 formed in the Late Carboniferous and at ca. 315 Ma in the Tacheng area.
- (2) The petrological data indicate that the andesites are similar to magnesian andesites with some adakitic geochemical characteristics and several of the basalt samples belong to Nb-enriched basalts. These volcanic rocks were derived from a metasomatized depleted mantle source in an island arc setting.
- (3) The Carboniferous sedimentary fill of the Balkhash–West Junggar remnant ocean basin can be divided into two stages. Early Carboniferous deep marine sediments covered the western Junggar region, whereas the Late Carboniferous sediments that filled the basin were dominated by shallow marine sediments. This sedimentary fill model resulted from accretionary processes

and was a response to Carboniferous arc-related tectonic evolution.

- (4) The unconformity between the Carboniferous and Lower Permian divides the Carboniferous–Early Permian strata into two tectonostratigraphic units. The Early Permian overlap on the Carboniferous strata and the transition from the Carboniferous marine to Early Permian terrigenous facies show that the Balkhash–Western Junggar remnant ocean basin closed during the Early Permian.

Acknowledgments

We are very grateful to the Editor-in-Chief Prof. M. Santosh for his constructive comments that significantly improved the original manuscript. We acknowledge Dr. Richard Glen, two anonymous referees and the Associate Editor Prof. Wenjiao Xiao for their critical and constructive comments. Xinjiang Oilfield Company kindly supplied drill core samples and part of the PSA data for the Carboniferous strata of the Tacheng Basin. We wish to thank Dr. Yuting Cao and Kaiyun Chen at Northwest University who helped us with the LA-ICP-MS zircon U–Pb analyses and Dr. Chaofeng Li and Qiannan Li for their help in carrying out the Sr–Nd isotopic analysis at the Institute of Geology and Geophysics, Chinese Academy of Sciences. This research was financially supported by the National Science and Technology Major Project (2011ZX05008-001, 2011ZX05002-

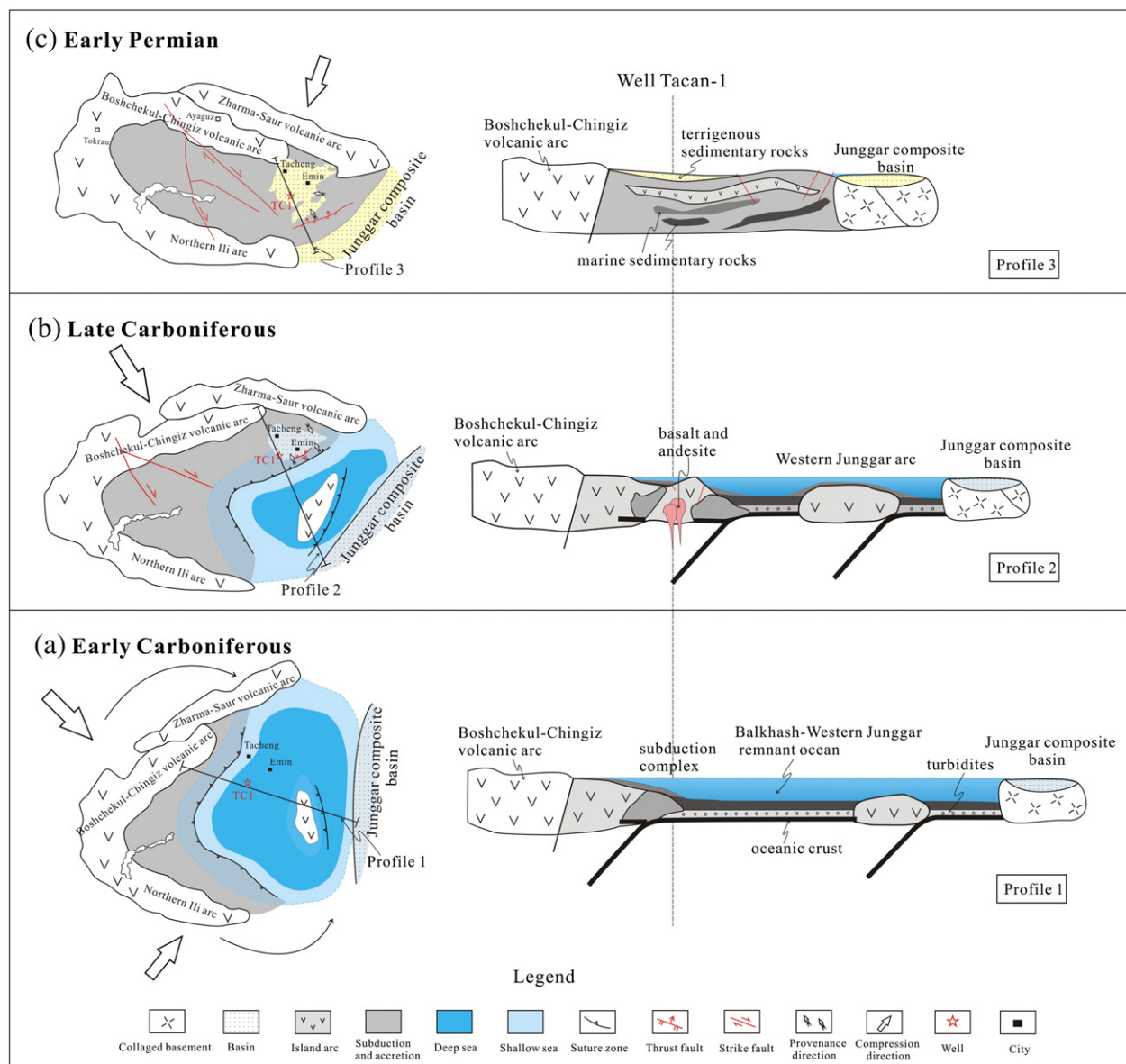


Fig. 19. Schematic diagrams illustrating the Carboniferous–Early Permian tectonic framework and filling evolution.

002), the National Natural Science Foundation of China (41272237, 40739906) and the Chinese State 973 Project (2011CB201100).

References

- Abrajevitch, A., Van der Voo, R., Levashova, N.M., Bazhenov, M.L., 2007. Paleomagnetic constraints on the paleogeography and orocinal bending of the Devonian volcanic arc in Kazakhstan. *Tectonophysics* 441, 67–84.
- Abrajevitch, A., Van der Voo, R., Bazhenov, M.L., Levashova, N.M., McCausland, P., 2008. The role of the Kazakhstan orocline in the late Paleozoic amalgamation of Eurasia. *Tectonophysics* 455, 61–76.
- Aguiló-Robles, A., Calmus, T., Benoit, M., Bellon, H., Maury, R., Cotten, J., Bourgois, J., Michaud, F., 2001. Late Miocene adakites and Nb-enriched basalts from Vizcaino Peninsula, Mexico: indicators of East Pacific Rise subduction below southern Baja California. *Geology* 29, 531–534.
- Allegre, C.J., Minster, J.F., 1978. Quantitative method of trace element behavior in magmatic processes. *Earth and Planetary Science Letters* 38, 1–25.
- Allen, M.B., Şengör, A.M., Natal'in, B.A., 1995. Junggar, Turfan and Alakol basins as Late Permian to Early Triassic extensional structures in a sinistral shear zone in the Altai orogenic collage, Central-Asia. *Journal of the Geological Society of London* 152, 327–338.
- An, F., Zhu, Y.F., 2009. SHRIMP U-Pb zircon ages of tuff in Baogutu formation and their geological significances. *Acta Petrologica Sinica* 25, 1437–1445 (in Chinese with English abstract).
- Andersen, T., 2002. Correction of common lead in U-Pb analysis that do not report ^{204}Pb . *Chemical Geology* 192, 59–79.
- Arndt, N.T., Jenner, G.A., 1986. Crustally contaminated komatiites and basalts from Kambalda, Western Australia. *Chemical Geology* 56, 229–255.
- Atherton, M.P., Petford, N., 1993. Generation of sodium-rich magmas from newly underplated basaltic crust. *Nature* 362, 144–146.
- Badarach, G., Cunningham, W.D., Windley, B.F., 2002. A new terrane subdivision for Mongolia: implications for the Phanerozoic crustal growth of Central Asia. *Journal of Asian Earth Sciences* 21, 87–110.
- BGMRXUAR (Bureau of Geology Mineral Resources of Xinjiang Uygur Autonomous Region), 1993. *Regional Geology of Xinjiang Uygur Autonomous Region*. People's Republic of China, Ministry of Geology and Mineral Resources. Geological Memoirs, Series 1, No. 32. Geological Publishing House, Beijing 6–206 (in Chinese).
- Bourdon, E., Eissen, J.P., Monzier, M., Robin, C., Martin, H., Cotton, J., Hall, M.L., 2002. Adakite-like lavas from Antisana volcano (Ecuador): evidence for slab melt metasomatism beneath the Andean Northern volcanic zone. *Journal of Petrology* 43, 199–217.
- Buckman, S., Aitchison, J.C., 2004. Tectonic evolution of Paleozoic terranes in West Junggar, Xinjiang, NW China. In: Malpas, J., Fletcher, C.J.N., Aitchison, J.C. (Eds.), *Aspects of the Tectonic Evolution of China: Geological Society of London, Special Publication*, 226, pp. 101–129.
- Buslov, M.M., Saphonova, I.Yu., Watanabe, T., Obut, O.T., Fujiwara, Y., Iwata, K., Semakov, N.N., Sugai, Y., Smirnova, L.V., Kazansky, A.Yu., 2001. Evolution of the Paleo-Asian Ocean (Altai-Sayan Region, Central Asia) and collision of possible Gondwanaderived terranes with the southern marginal part of the Siberian continent. *Geoscience Journal* 5, 203–224.
- Buslov, M.M., Watanabe, T., Fujiwara, Y., Iwata, K., Smirnova, L.V., Safonova, I.Yu., Semakov, N.N., Kiryanova, A.P., 2004. Late Paleozoic faults of the Altai region, Central Asia: tectonic pattern and model of formation. *Journal of Asian Earth Sciences* 23, 655–671.

- Cabanis, B., Lecolle, M., 1989. La diagramme La/10-Y/15-Nb/8, Un outil pour la discrimination des séries volcaniques et la mise en évidence des processus de mélange et/ou de contamination crustale. *Comptes Rendus de l' Académie des Sciences Serie II* 309, 2023–2029.
- Calmus, T., Aguillón-Robles, A., Maury, R.C., Bellon, H., Benoit, M., Cotten, J., Bourgois, J., Michaud, F., 2003. Spatial and temporal evolution of basalts and magnesian andesites ("bajaites") from Baja California, Mexico: the role of slab melts. *Lithos* 66, 77–103.
- Castillo, P.R., Solidum, R.U., Punongbayan, R.S., 2002. Origin of high field strength element enrichment in the Sulu Arc, southern Philippines, revisited. *Geology* 30, 707–710.
- Che, Z.C., Liu, L., Liu, H.F., Luo, J.H., 1996. Review on the ancient Yili Rift, Xinjiang, China. *Acta Petrologica Sinica* 12, 478–490 (in Chinese with English abstract).
- Chen, B., Arakawa, Y., 2005. Elemental and Nd-Sr isotopic geochemistry of granitoids from the West Junggar foldbelt (NW China), with implications for Phanerozoic continental growth. *Geochimica et Cosmochimica Acta* 69, 1307–1320.
- Chen, B., Jahn, B.M., 2004. Genesis of post-collisional granitoids and basement nature of the Junggar Terrane, NW China: Nd-Sr isotope and trace element evidence. *Journal of Asian Earth Sciences* 23, 691–703.
- Chen, B., Zhu, Y.F., 2011. Petrology, geochemistry and zircon U-Pb chronology of gabbro in Darbuit ophiolitic mélange, Xinjiang. *Acta Petrologica Sinica* 27, 1746–1758 (in Chinese with English abstract).
- Chen, D.L., Liu, L., Che, Z.C., Luo, J.H., 2001a. Geochemical characteristics and tectonic implication of Carboniferous volcanites in the Luotugou area of Middle Tianshan. *Acta Petrologica Sinica* 17, 378–384 (in Chinese with English abstract).
- Chen, F.K., Siebel, W., Satir, M., 2001b. Zircon U-Pb and Pb-isotope fractionation during stepwise HF acid leaching and geochronological implications. 11th Meeting of the European Union of Geosciences (EUG), Strasbourg, France, pp. 155–164.
- Chen, Y., Sun, M.S., Zhang, X.L., 2006. SHRIMP U-Pb dating of zircons from quartz diorite at the southeast side of the Baerkule fault, western Junggar, Xinjiang, China. *Geological Bulletin of China* 25, 992–994 (in Chinese with English abstract).
- Chen, J.F., Han, B.F., Ji, J.Q., Zhang, L., Xu, Z., He, G.Q., Wang, T., 2010. Zircon U-Pb ages and tectonic implications of Paleozoic plutons in northern West Junggar, North Xinjiang, China. *Lithos* 115, 137–152.
- Chen, S., Guo, Z.J., Pe-Piper, G., Zhu, B.B., 2013. Late Paleozoic peperites in West Junggar, China, and how they constrain regional tectonic and palaeoenvironmental setting. *Gondwana Research* 23, 666–681.
- Choulet, F., Faure, M., Cluzel, D., Chen, Y., Lin, W., Wang, B., 2012. From oblique accretion to transposition in the evolution of the Altai collage: new insights from West Junggar, northwestern China. *Gondwana Research* 21, 530–547.
- Coleman, R.G., 1989. Continental growth of Northwest China. *Tectonics* 8, 621–635.
- Collins, A.Q., Degtyarev, K.E., Levashova, N.M., Bazhenov, M.L., Van der Voo, R., 2003. Early Paleozoic paleomagnetism of East Kazakhstan: implications for paleolatitudinal drift of tectonic elements within the Ural-Mongolia belt. *Tectonophysics* 377, 229–247.
- Condie, K.C., 1994. Greenstones through time. In: Condie, K.C. (Ed.), *Archean Crustal Evolution*. Elsevier, Amsterdam, pp. 85–120.
- Dahlstrom, C.D.A., 1969. Balanced cross sections. *Canadian Journal of Earth Sciences* 6, 743–757.
- Defant, M.J., Drummond, M.S., 1990. Derivation of some modern arc magmas by melting of young subduction lithosphere. *Nature* 347, 662–665.
- Defant, M.J., Drummond, M.S., 1993. Mount St. Helens: potential example of the partial melting of the subducted lithosphere in a volcanic arc. *Geology* 21, 547–550.
- Defant, M.J., Clark, J.K., Stewart, R.H., Drummond, M.S., de Boer, J.Z., Maury, R.C., Bellon, H., Jackson, T.E., Restrepo, J.F., 1991. Andesite and dacite genesis via contrasting processes: the geology and geochemistry of El Valle Volcano, Panama. *Contributions to Mineralogy and Petrology* 106, 309–324.
- Defant, M.J., Jackson, T.E., Drummond, M.S., de Boer, J.Z., Bellon, H., Feigenson, M.D., Maury, R.C., Stewart, R.H., 1992. The geochemistry of young volcanism throughout western Panama and southern Costa Rica, an overview. *Journal of the Geological Society of London* 149, 569–579.
- Defant, M.J., Xu, J.F., Kepezhinskis, P., Wang, Q., Zhang, Q., Xiao, L., 2002. Adakite: some variations on a theme. *Acta Petrologica Sinica* 18, 129–142.
- Dobretsov, N.I., Buslov, M.M., Uchio, Y., 2004. Fragments of oceanic islands in accretion-collision areas of Gorny Altai and Salair, southern Siberia, Russia: early stages of continental crustal growth of the Siberian continent in Vendian-Early Cambrian time. *Journal of Asian Earth Sciences* 23, 673–690.
- Feng, Y.M., 1987. Characteristics of ancient plate tectonics in West Junggar. *Bulletin of Xi'an Institute of Geology and Minerals Resources, Chinese Academy of Geological Sciences*, 18, pp. 141–160 (in Chinese with English abstract).
- Feng, Y., Coleman, R.G., Tilton, G., Xiao, X., 1989. Tectonic evolution of the West Junggar region, Xinjiang, China. *Tectonics* 8, 729–752.
- Feng, Y.M., Zhu, B.Q., Xiao, X.C., Yan, B.G., Wang, G.R., Zhang, Y.P., 1991. Tectonic evolution of the West Junggar, Xinjiang, China. In: Xiao, X.C., Tang, Y.Q. (Eds.), *Tectonic Evolution of the Southern Margin of the Paleo-Asian Composite Megasuture*. Beijing Scientific and Technical Publishing House, Beijing, pp. 66–91.
- Filippova, I.B., Bush, V.A., Didenko, A.N., 2001. Middle Paleozoic subduction belts: the leading factor in the formation of the Central Asian fold-and-thrust belt. *Russian Journal of Earth Sciences* 3, 405–426.
- Gao, J., Klemd, R., 2000. Eclogite occurrences in the Southern Tianshan high-pressure belt, Xinjiang, Western China. *Gondwana Research* 3, 33–38.
- Gao, J., Tang, Y.Q., Zhao, M., Wang, J., Wu, H.Q., 1994. Blueschists discovered in Kumishi, South Tianshan and their tectonic significance. In: Coleman, R.G. (Ed.), *Reconstruction of the Paleo-Asian Ocean: Proceeding of the 29th International Geological Congress. Part B*. VSP, Utrecht, The Netherlands, pp. 115–118.
- Gao, J., He, G.Q., Li, M.S., Xiao, X.C., Tang, Y.Q., 1995. The mineralogy, petrology, metamorphic P-T-dt trajectory and exhumation mechanism of blueschists, south Tianshan, northwestern China. *Tectonophysics* 250, 151–168.
- Gao, J., Li, M., Xiao, X., Tang, Y., He, G., 1998. Paleozoic tectonic evolution of the Tianshan orogen, northwestern China. *Tectonophysics* 287, 213–231.
- Gao, S., Ling, W.L., Qiu, Y.M., Lian, Z., Hartmann, G., Simon, K., 1999. Contrasting geochemical and Sm-Nd isotopic compositions of Archean metasediments from the Kongling high-grade terrain of the Yangtze craton: evidence for cratonic evolution and redistribution of REE during crustal anatexis. *Geochimica et Cosmochimica Acta* 63, 2071–2088.
- Geng, H.Y., Sun, M., Yuan, C., Xiao, W.J., Xian, W.S., Zhao, G.C., Zhang, L.F., Wong, K., Wu, F.Y., 2009. Geochemical, Sr-Nd and zircon U-Pb-Hf isotopic studies of Late Carboniferous magmatism in the Western Junggar, Xinjiang: implications for ridge subduction? *Chemical Geology* 266, 364–389.
- Geng, H.Y., Sun, M., Yuan, C., Zhao, G.C., Xiao, W.J., 2011. Geochemical and geochronological study of early Carboniferous volcanic rocks from the West Junggar: petrogenesis and tectonic implications. *Journal of Asian Earth Sciences* 42, 854–866.
- Gu, P.Y., Li, Y.J., Zhang, B., Tong, L.L., Wang, J.N., 2009. LA-ICP-MS zircon U-Pb dating of gabbro in the Darbuit ophiolite, West Junggar, China. *Acta Petrologica Silica* 25, 1364–1372 (in Chinese with English abstract).
- Guo, H.L., Zhu, R.K., Shao, L.Y., He, D.B., Luo, Z.G., 2002. Lithofacies palaeogeography of the Carboniferous in Northwest China. *Journal of Palaeogeography* 4, 25–35.
- Guo, L.S., Liu, Y.L., Wang, Z.H., Song, D., Xu, J.F., Su, L., 2010. The zircon U-Pb LA-ICP-MS geochronology of volcanic rocks in Baogutu areas, western Junggar. *Acta Petrologica Sinica* 26, 471–477 (in Chinese with English abstract).
- Han, B.F., Ji, J.Q., Song, B., Chen, L.H., Zhang, L., 2006. Late Paleozoic vertical growth of continental crust around the Junggar Basin, Xinjiang, China (Part I): timing of post-collisional plutonism. *Acta Petrologica Sinica* 22, 1077–1086 (in Chinese with English abstract).
- Han, B.F., Guo, Z.J., Zhang, Z.C., Zhang, L., Chen, J.F., Song, B., 2010. Age, geochemistry, and tectonic implications of a late Paleozoic stitching pluton in the North Tian Shan suture zone, western China. *Geological Society of America Bulletin* 122, 627–640.
- Hart, S.R., 1988. Heterogeneous mantle domains: signature, genesis and mixing chronologies. *Earth and Planetary Science Letters* 90, 273–296.
- He, G.Q., Xu, X., 2003. The plate tectonic division of Chinese Tianshan—a consideration to Kazakhstan Plate. In: He, G.Q., Xu, X. (Eds.), *The Chinese Xinjiang Tianshan Tectonic and Mineral Proceedings*. Geological Publishing House, Beijing (in Chinese with English abstract).
- He, G.Q., Li, M.S., Liu, D.Q., Tang, Y.L., Zhou, R.H., 1994. *Paleozoic Crustal Evolution and Mineralization in Xinjiang of China*. Xinjiang People's Publishing House, Urumqi (Hong Kong: Educational and Cultural Press LTD, 1–437 (in Chinese with English abstract)).
- He, G.Q., Chen, S.D., Xu, X., Li, J.Y., Hao, J., 2004. An introduction to tectonic map of Xinjiang and its neighboring area (1: 250 000). Geological Publishing House, Beijing. 65 pp.
- He, D.F., Li, D., Fan, C., Yang, X.F., 2013. Geochronology, geochemistry and tectonostratigraphy of Carboniferous strata of the deepest Well Moshen-1 in the Junggar Basin, Northwest China: insights into the continental growth of Central Asia. *Gondwana Research* 24, 560–577.
- Helo, C., Hegner, E., Kröner, A., Badarch, G., Tomurtogoo, O., Windley, B.F., Dulski, P., 2006. Geochemical signature of Paleozoic accretionary complexes of the Central Asian Orogenic Belt in South Mongolia: constraints on arc environments and crustal growth. *Chemical Geology* 227, 236–257.
- Huang, F., Li, S., Dong, F., He, Y., Chen, F., 2008. High-Mg adakitic rocks in the Dabie orogen, central China: implications for foudering mechanism of lower continental crust. *Chemical Geology* 255, 1–13.
- Irvine, T.N., Baragar, W.R.A., 1971. A guide to the chemical classification of the common volcanic rocks. *Canada Journal of Earth Science* 8, 523–548.
- Jahn, B.M., Natal'in, B.A., Windley, B.F., Dobretsov, N., 2004. Phanerozoic continental growth in Central Asia. *Journal of Asian Earth Sciences* 23, 599–603.
- Jian, P., Liu, D.Y., Shi, Y.R., Zhang, F.Q., 2005. SHRIMP dating of SSZ ophiolites from northern Xinjiang Province, China: implications for generation of oceanic crust in the Central Asian orogenic belt. In: Sklyarov, E.V. (Ed.), *Structural and Tectonic Correlation across the Central Asia Orogenic Collage: North-Eastern Segment; Guidebook and Abstract Volume of the Siberian Workshop ICP-480*, 246. Institute of the Earth Crust, Siberian Branch of Russian Academy of Sciences, Irkutsk.
- Jin, H.J., Li, Y.C., 1999. Carboniferous biogenic sedimentary structures on the northwestern margin of Jungar basin. *Chinese Science Bulletin* 44, 368–372.
- Kepezhinskis, P.K., Defant, M.J., Drummond, M.S., 1996. Progressive enrichment of island arc mantle by melt-peridotite interaction inferred from Kamchatka xenoliths. *Geochimica et Cosmochimica Acta* 60, 1217–1229.
- Khain, E.V., Bibikova, E.V., Kröner, A., Zhuravlev, D.Z., Sklyarov, E.V., Fedotova, A.A., Kravchenko-Berezinoy, I.R., 2002. The most ancient ophiolite of Central Asian fold belt: U-Pb and Pb-Pb zircon ages for the Dunzhungur Complex, Eastern Sayan, Siberia, and geodynamic implications. *Earth and Planetary Science Letters* 199, 311–325.
- Khain, E.V., Bibikova, E.V., Salnikova, E.B., Kröner, A., Gibsher, A.S., Didenko, A.N., Degtyarev, K.E., Fedotova, A.A., 2003. The Paleo-Asian ocean in the Neoproterozoic and early Palaeozoic: new geochronologic data and palaeotectonic reconstructions. *Precambrian Research* 122, 329–358.
- Kröner, A., Windley, B.F., Badarch, G., Tomurtogoo, O., Hegner, E., Jahn, B.M., Gruschka, S., Khain, E.V., Demoux, A., Wingate, M.T.D., 2007. Accretionary growth and crust formation in the Central Asian Orogenic Belt and comparison with the Arabian–Nubian–Shield. *Geological Society America, Memoir* 200, 181–209.
- Kröner, A., Hegner, E., Lehmann, B., Heinhorst, J., Wingate, M.T.D., Liu, D.Y., Ermelov, P., 2008. Paleozoic arc magmatism in the Central Asian Orogenic Belt of Kazakhstan: SHRIMP zircon ages and whole-rock Nd isotopic systematics. *Journal of Asian Earth Sciences* 32, 118–130.
- Kuibida, M.L., Kruk, N.N., Vladimirov, A.G., Polyanskii, N.V., Nikolaeva, I.V., 2009. U-Pb isotopic age, composition, and sources of the plagiogranoites of the Kalba Range, Eastern Kazakhstan. *Doklady Earth Sciences* 424, 72–76.

- Le Maitre, R.W., Bateman, P., Dudek, A., Keller, J., Lameyre Le Bas, M.J., Sabine, P.A., Schmid, R., Sorensen, H., Streckeisen, A., Woolley, A.R., Zanettin, B., 1989. *A Classification of Igneous Rocks and Glossary of Terms*. Blackwell, Oxford.
- Levashova, N.M., Mikolaichuk, A.V., McCausland, P.J.A., Bazhenov, M.L., Van der Voo, R., 2007. Devonian paleomagnetism of the North Tien Shan: implications for the Middle–Late Paleozoic paleogeography of Eurasia. *Earth and Planetary Science Letters* 257, 104–120.
- Li, J.Y., Jin, H.J., 1989. The trace fossils discovery and its environment significance in Carboniferous turbidite series, the northwest border of Zhung'er basin, Xinjiang. *Scientia Geologica Sinica* 63, 9–15.
- Li, Y.J., Sun, L.D., Wu, H.R., Wang, G.L., Yang, C.S., Peng, G.X., 2005. Permo-Carboniferous radiolarian from the Wupatarkan Group, western terminal of Chinese South Tianshan. *Chinese Journal of Geology* 40, 220–226 (in Chinese with English abstract).
- Li, D., He, D.F., Tang, Y., Fan, C., Kong, Y.H., 2012. Genesis of Early Carboniferous volcanic rocks of the Di'an uplift in Junggar Basin: constraints to the closure time of Kalamaili ocean. *Acta Petrologica Sinica* 28, 2340–2354 (in Chinese with English abstract).
- Liu, X.J., Xu, J.F., Wang, S.Q., Hou, Q.Y., Bai, Z.H., Lei, M., 2009. Geochemistry and dating of E-MORB type mafic rocks from Dalabute ophiolite in West Junggar, Xinjiang and geological implications. *Acta Petrologica Sinica* 25, 1373–1389 (in Chinese with English abstract).
- Ludden, J., Gelinas, L., Trudel, P., 1982. Archean metavolcanics from the Rouyn-Noranda district, Abitibi greenstone belt, Quebec. 2. Mobility of trace elements and petrogenetic constraints. *Canadian Journal of Earth Sciences* 19, 2276–2287.
- Ludwig, K.R., 2003. Isoplot/Ex version 2.49. A Geochronological Toolkit for Microsoft Excel. Special Publication No., 1a. Berkeley Geochronology Center, Berkeley, pp. 1–56.
- Manyo, S., Maboko, M.A.H., Nakamura, E., 2007. The geochemistry of high-Mg andesite and associated adakitic rocks in the Musoma–Mara Greenstone Belt, northern Tanzania: possible evidence for Neoproterozoic ridge subduction? *Precambrian Research* 159, 241–259.
- Mao, Q.G., Xiao, W.J., Fang, H.T., Wang, J.B., Han, C.M., Sun, M., Yuan, C., 2012. Late Ordovician to early Devonian adakites and Nb-enriched basalts in the Liuyuan area, Beishan, NW China: implications for early Paleozoic slab-melting and crustal growth. *Gondwana Research* 22, 534–553.
- Martin, H., 1999. Adakitic magmas: modern analogues of Archaean granitoids. *Lithos* 46, 411–429.
- Martin, H., Smithies, R.H., Rapp, R., Moyen, J.F., Champion, D., 2005. An overview of adakite, tonalite–trondhjemite–granodiorite (TTG), and sanukitoid: relationships and some implications for crustal evolution. *Lithos* 79, 1–24.
- Middlemost, E.A.K., 1975. The basalt clan. *Earth Sciences Review* 11, 337–364.
- Mossakovskiy, A.A., Ruzhentsev, S.V., Samygin, S.G., Kheraskova, T.N., 1993. The Central Asian fold belt: geodynamic evolution and formation history. *Geotectonics* 26, 455–473.
- Muir, R.J., Weaver, S.D., Bradshaw, J.D., Eby, G.N., Evans, J.A., 1995. Geochemistry of the Cretaceous Scarpnorthern Plint Batholith, New Zealand: granitoid magmas formed by melting of mafic lithosphere. *Journal of the Geological Society of London* 152, 689–701.
- Nesbitt, H.W., Young, G.M., 1982. Early Proterozoic climates and plate motions inferred from major element chemistry of lutes. *Nature* 299, 715–717.
- Niu, H.C., Shan, Q., Yu, X.Y., Zhang, B., Luo, Y., Yang, W.B., 2009. Geochemistry of the Nb-enriched basalt and its significances in Zaheba ophiolite mélange. *Acta Petrologica Sinica* 25, 916–924 (in Chinese with English abstract).
- Pearce, J.A., Cann, J., 1973. Tectonic setting of basic volcanic rocks determined using trace element analyses. *Earth and Planetary Science Letters* 19, 290–300.
- Pearce, J.A., Mei, H.J., 1990. Lasa to Geermu volcanic rocks. In: Team, China–Britain Qinghai-Tibet Plateau Geological Comprehensive Scientific Expedition (Ed.), *Qinghai-Tibet Plateau Geological Evolution*. Science Press, Beijing, pp. 174–205 (in Chinese with English abstract).
- Pecceirillo, A., Taylor, S.R., 1976. Geochemistry of Eocene calc-alkaline volcanic rocks from the Kastamonu area, northern Turkey. *Contributions to Mineralogy and Petrology* 58, 130–143.
- Petford, N., Atherton, M., 1996. Na-rich partial melts from newly underplated basaltic crust: the Cordillera Blanca Batholith, Peru. *Journal of Petrology* 37, 1491–1521.
- Prouteau, G., Scaillet, B., Pichavent, M., Maury, R., 2001. Evidence for mantle metasomatism by hydrous silicic melts derived from subducted oceanic crust. *Nature* 410, 197–200.
- Rapp, R.P., Watson, E.B., 1995. Dehydration melting of metabasalt at 8–32 kbar: implications for continental growth and crust–mantle recycling. *Journal of Petrology* 36, 891–931.
- Rapp, R.P., Shimizu, N., Norman, M.D., Applegate, G.S., 1999. Reaction between slab-derived melts and peridotite in the mantle wedge: experimental constraints at 3.8 GPa. *Chemical Geology* 160, 335–356.
- Redman, I.S., Keays, R.R., 1985. Archean volcanism in the eastern Goldfields province, Western Australia. *Precambrian Research* 30, 113–152.
- Rudnick, R.L., Gao, S., 2003. Composition of the continental crust. In: Rudnick, R.L. (Ed.), *The Crust*, vol. 3. Elsevier, pp. 1–64.
- Safonova, I.Yu., Buslov, M.M., Iwata, K., Kokh, D.A., 2004. Fragments of Vendian–Early Carboniferous oceanic crust of the Paleo-Asian Ocean in foldbelts of the Altai-Sayan region of Central Asia: geochemistry, biostratigraphy and structural setting. *Gondwana Research* 7, 771–790.
- Sajona, F.G., Maury, R.C., Bellon, H., Cotton, J., Defant, M.J., Pubbellier, M., Rangin, C., 1993. Initiation of subduction and the generation of slab melts in western and eastern Mindanao, Philippines. *Geology* 21, 1007–1010.
- Sajona, F.G., Maury, R.C., Bellon, H., Cotton, J., Defant, M., 1996. High field strength element enrichment of Pliocene–Pleistocene island arc basalts, Zamboanga Peninsula, western Mindanao (Philippines). *Journal of Petrology* 37, 693–726.
- Samygin, S.G., Ruzhentsev, S.V., Pospelov, I.I., Mossakovskiy, A.A., Sharkova, T.T., Aristov, V.A., 1997. Variscan Junggar transform zone: an experience of revelation. *Tectonic and Geodynamics Basis*. Moscow (in Russian with English abstract).
- Santosh, M., Maruyama, S., Sato, K., 2009. Anatomy of a Cambrian suture in Gondwana: Pacific-type orogeny in southern India? *Gondwana Research* 16, 321–341.
- Selmann, R., Porter, T.M., 2005. The porphyry Cu-Au/Mo deposits of central Eurasia I. Tectonic, geologic and metallogenic setting, and significant deposits. In: Porter, T.M. (Ed.), *Super Porphyry Copper and Gold Deposits: A Global Perspective*, vol. 2. PGC Publishing, Adelaide, pp. 467–512.
- Sen, C., Dunn, T., 1994. Dehydration melting of a basaltic composition amphibolite at 1.5 and 2.0 GPa: implications for the origin of adakites. *Contributions to Mineralogy and Petrology* 117, 394–409.
- Sengör, A.M.C., Natal'In, B.A., 1996. Turkin-type orogeny and its role in the making of the continental crust. *Annual Review of Earth and Planetary Sciences* 24, 263–337.
- Sengör, A.M.C., Natal'In, B.A., Burtman, V.S., 1993. Evolution of the Altai tectonic collage and Paleozoic crustal growth in Eurasia. *Nature* 364, 299–307.
- Shen, Y.C., Jin, C.W., 1993. Magmatism and gold mineralization in Western Junggar. *Beijing Science Press* 113–172 (in Chinese with English abstract).
- Shen, P., Shen, Y.C., Liu, T.B., Meng, L., Dai, H.W., Yang, Y.H., 2009. Geochemical signature of porphyries in the Baogutu porphyry copper belt, western Junggar, NW China. *Gondwana Research* 16, 227–242.
- Shen, P., Shen, Y.C., Wang, J.B., Zhu, H.P., Wang, L.J., Meng, L., 2010. Methane-rich fluid evolution of the Baogutu porphyry Cu–Mo–Au deposit, Xinjiang, NW China. *Chemical Geology* 275, 78–98.
- Shen, P., Shen, Y.C., Li, X.H., Pan, H.D., Zhu, H.P., Meng, L., Dai, H.W., 2012. Northwestern Junggar Basin, Xiemisitai Mountains, China: a geochemical and geochronological approach. *Lithos* 140–141, 103–118.
- Shirey, S.B., Harson, G.N., 1984. Mantle-derived Archean monzodiorites and trachyandesites. *Nature* 310, 222–224.
- Smithies, R.H., 2000. The Archean tonalite–trondhjemite–granodiorite (TTG) series is not an analogue of Cenozoic adakite. *Earth and Planetary Science Letters* 182, 115–125.
- Smithies, R.H., Champion, D.C., 2000. The Archean high-Mg diorite suite: links to tonalite–trondhjemite–granodiorite magmatism and implications for Early Archean crustal growth. *Journal of Petrology* 41, 1653–1671.
- Smithies, R.H., Champion, D.C., Sun, S.S., 2004. Evidence for early LREE-enriched mantle source regions: diverse magmas from the 3.0 Ga Mallina basin, Pilbara craton, NW Australia. *Journal of Petrology* 45, 1515–1537.
- Smithies, R.H., Van Kranendonka, M.J., Champion, D.C., 2007. The Mesoarchean emergence of modern-style subduction. *Gondwana Research* 11, 50–68.
- Springer, W., Seck, H.A., 1997. Partial fusion of basic granulites at 5 to 15 kbar: implications for the origin of TTG magmas. *Contributions to Mineralogy and Petrology* 127, 30–45.
- Stern, C.R., Hanson, G., 1991. Archean high-Mg frondiorites: a derivative of light rare earth element enriched monzodiorite of mantle origin. *Journal of Petrology* 32, 201–238.
- Stern, C.R., Kilian, R., 1996. Role of the subducted slab, mantle wedge and continental crust in the generation of adakites from the Austral Volcanic Zone. *Contributions to Mineralogy and Petrology* 123, 263–281.
- Stern, R.J., Kohut, E., Bloomer, S.H., Leybourne, M., Fouch, M., Vervoort, J., 2006. Subduction factory processes beneath the Guguan cross-chain, Mariana Arc: no role for sediments, are serpentinites important? *Contributions to Mineralogy and Petrology* 151, 202–221.
- Su, Y.P., Tang, H.F., Hou, G.S., Liu, C.Q., 2006. Geochemistry of aluminous A-type granites along Darabute tectonic belt in West Junggar, Xinjiang. *Geochemistry* 35, 1–5 (in Chinese with English abstract).
- Sun, S.S., McDonough, W.F., 1989. Chemical and isotopic systematics of ocean basalts: implication for mantle composition and processes. In: Saunders, A.D., Norry, M.J. (Eds.), *Magmatism in Ocean Basins*. Geological Society Special Publication, 42, pp. 313–345.
- Tang, G.J., Wang, Q., Zhao, Z.H., Wyman, D.A., Chen, H.H., Jia, X.H., Jiang, Z.Q., 2009. Geochronology and geochemistry of the ore-bearing porphyries in the Baogutu area (Western Junggar): petrogenesis and their implications for tectonics and Cu–Au mineralization. *Earth Science–Journal of China University of Geosciences* 34, 56–74.
- Tang, G.J., Wang, Q., Wyman, D.A., Li, Z.X., Zhao, Z.H., Jia, X.H., Jiang, Z.Q., 2010. Ridge subduction and crustal growth in the Central Asian Orogenic Belt: evidence from Late Carboniferous adakites and high-Mg diorites in the western Junggar region, northern Xinjiang (west China). *Chemical Geology* 277, 281–300.
- Tang, G.J., Wang, Q., Wyman, D.A., Li, Z.X., Zhao, Z.H., Yang, Y.H., 2012a. Late Carboniferous high $\epsilon_{\text{Nd}}(\text{t})$ – $\epsilon_{\text{Hf}}(\text{t})$ granitoids, enclaves and dikes in western Junggar, NW China: ridge–subduction-related magmatism and crustal growth. *Lithos* 140–141, 86–102.
- Tang, G.J., Wyman, D.A., Wang, Q., Li, J., Li, Z.X., Zhao, Z.H., Sun, W.D., 2012b. Asthenosphere–lithosphere interaction triggered by a slab window during ridge subduction: trace element and Sr–Nd–Hf–Os isotopic evidence from Late Carboniferous tholeiites in the western Junggar area (NW China). *Earth and Planetary Science Letters* 329–330, 84–96.
- Tatsumi, Y., Hanyu, T., 2003. Geochemical modeling of dehydration and partial melting of subducting lithosphere: toward a comprehensive understanding of high-Mg andesite formation in the Setouchi volcanic belt, SW Japan. *Geochemistry, Geophysics, Geosystems* 4, 1081. <http://dx.doi.org/10.1029/2003GC000530>.
- Taylor, S.R., McLennan, S.M., 1985. *The Continental Crust: its Composition and Evolution*. Blackwell, Oxford.
- Turner, S., Hawkesworth, C., Rogers, N., King, P., 1997. U–Th isotope disequilibrium and ocean island basalt generation in the Azores. *Chemical Geology* 139, 145–164.
- Van der Voo, R., 2004. Paleomagnetism, oroclines and the growth of the continental crust. *GSA Today* 14 (12), 4–9.

- Vladimirov, A.G., Kruk, N.N., Khromykh, S.V., Polyansky, O.P., Chernov, V.V., Vladimirov, V.G., Travin, A.V., Babin, G.A., Kuibida, M.L., Khomyakov, V.D., 2008. Permian magmatism and lithospheric deformation in the Altai caused by crustal and mantle thermal processes. *Russian Geology and Geophysics* 49, 468–479.
- Wang, W.G., Sun, Y.L., 2005. Geological features and guides for exploration of the Haxi Gold Deposit Xinjiang. *Xinjiang Geology* 25, 31–35 (in Chinese with English abstract).
- Wang, R., Zhu, Y.F., 2007. Geology of the Baobei gold deposit in Western Junggar and zircon SHRIMP age of its wall-rocks, Western Junggar (Xinjiang, NW China). *Geological Journal of China Universities* 13, 590–602 (in Chinese with English abstract).
- Wang, Z.H., Sun, S., Li, J.L., Hou, Q.L., Qin, K.Z., Xiao, W.J., Hao, J., 2003. Paleozoic tectonic evolution of the northern Xinjiang, China: geochemical and geochronological constraints from the ophiolites. *Tectonics* 22, 1014. <http://dx.doi.org/10.1029/2002TC001396>.
- Wang, Q., Xu, J.F., Jian, P., Bao, Z.W., Zhao, Z.H., Li, C.W., Xiong, X.L., Ma, J.L., 2006. Petrogenesis of adakitic porphyries in an extensional tectonic setting: Dexing, South China: implications for the genesis of porphyry copper mineralization. *Journal of Petrology* 47, 119–144.
- Wang, Q., Wyman, D.A., Zhao, Z.H., Xu, J.F., Zheng, H.B., Xiong, X.L., Dai, D.X., Li, H.C., Chu, Z.Y., 2007. Petrogenesis of Carboniferous adakites and Nb-enriched arc basalts in the Altay area, northern Tianshan range (western China): implications for Phanerozoic crustal growth in the central Asia orogenic belt. *Chemical Geology* 236, 42–64.
- Wang, Q., Wyman, D.A., Xu, J.F., Dong, Y., Vasconcelos, P.M., Pearson, N., Wang, Y., Dong, H., Li, C., Yu, Y., Zhu, T., Feng, X., Zhang, Q., Zi, F., Chu, Z., 2008. Eocene melting of subducting continental crust and early uplifting of central Tibet: evidence from central-western Qiangtang high-K calc-alkaline andesites, dacites and rhyolites. *Earth and Planetary Science Letters* 272, 158–171.
- Winchester, J.A., Floyd, P.A., 1977. Geochemical discrimination of different magma series and their differentiation products using immobile elements. *Chemical Geology* 20, 325–343.
- Windley, B.F., Alexeev, D., Xiao, W., Kröner, A., Badarch, G., 2007. Tectonic models for accretion of the Central Asian Orogenic Belt. *Journal of the Geological Society (London)* 164, 31–47.
- Wood, D.A., 1980. The application of a Th–Hf–Ta diagram to problems of tectonomagmatic classification and to establishing the nature of crustal contamination of basaltic lavas of the British Tertiary volcanic province. *Earth and Planetary Science Letters* 50, 11–30.
- Wood, D.A., Marsh, N.G., Tarney, J., Joron, L.J., Fryer, P., Treuil, M., 1981. Geochemistry of igneous rocks recovered from a transect across the Mariana trough, arc, fore-arc, and trench, sites 453 through 461, Deep Sea Drilling Project Leg 60. In: Husson, D.M. (Ed.), *Initial Reports of the Deep Sea Drilling Project*, 60, pp. 611–645.
- Woodward, N.B., Boyer, S.E., Suppe, J., 1989. Balanced geological cross sections: an essential technique in geological research and exploration. *Short Course in Geology*. AGU, Washington, D.C. 132.
- Wyman, D.A., Ayer, J.A., Devaney, J.R., 2000. Niobium-enriched basalts from the Wabigoon subprovince, Canada: evidence for adakitic metasomatism above an Archean subduction zone. *Earth and Planetary Science Letters* 179, 21–30.
- Xia, L.Q., Xu, X.Y., Xia, Z.C., Li, X.M., Ma, Z.P., Wang, L.S., 2004a. Petrogenesis of Carboniferous rift-related volcanic rocks in the Tianshan, northwestern China. *Geological Society of America Bulletin* 116, 419–433.
- Xia, L.Q., Xia, Z.C., Xu, X.Y., Li, X.M., Ma, Z.P., Wang, L.S., 2004b. Carboniferous Tianshan large igneous province and mantle plume. *Geological Bulletin of China* 23, 903–910 (in Chinese with English abstract).
- Xiao, W.J., Windley, B.F., Hao, J., Zhai, M.G., 2003. Accretion leading to collision and the Permian Solonker suture, Inner Mongolia, China: termination of the Central Asian Orogenic Belt. *Tectonics* 22, 1069. <http://dx.doi.org/10.1029/2002TC001484>.
- Xiao, W.J., Han, C.M., Yuan, C., Sun, M., Lin, S.F., Chen, H.L., Li, Z.L., Li, J.L., Sun, S., 2008. Middle Cambrian to Permian subduction-related accretionary orogenesis of North Xinjiang, NW China: implications for the tectonic evolution of Central Asia. *Journal of Asian Earth Sciences* 32, 102–117.
- Xiao, W.J., Windley, B.F., Yuan, C., Sun, M., Han, C.M., Lin, S.F., Chen, H.L., Yan, Q.R., Liu, D.Y., Qin, K.Z., Li, J.L., Sun, S., 2009. Paleozoic multiple subduction–accretion processes of the southern Altaiids. *American Journal of Science* 309, 221–270.
- Xiao, W.J., Huang, B.C., Han, C.M., Sun, S., Li, J.L., 2010. A review of the western part of the Altaiids: a key to understanding the architecture of accretionary orogens. *Gondwana Research* 18, 253–273.
- Xiao, W.J., Windley, B.F., Allen, M.B., Han, C.M., 2013. Paleozoic multiple accretionary and collisional tectonics of the Chinese Tianshan orogenic collage. *Gondwana Research* 23, 1316–1341.
- Xiong, X.L., Cai, Z.Y., Niu, H.C., Chen, Y.B., Wang, Q., Zhao, Z.H., Wu, J.H., 2005. The late Paleozoic adakites in eastern Tianshan area and their metallogenetic significance. *Acta Petrologica Sinica* 21, 967–976 (in Chinese with English abstract).
- Xu, Z., Han, B.F., Ren, R., Zhou, Y.Z., Zhang, L., Chen, J.F., Su, L., Li, X.H., Liu, D.Y., 2012. Ultramafic–mafic melange, island arc and post-collisional intrusions in the Mayile Mountain, West Junggar, China: implications for Paleozoic intra-oceanic subduction–accretion process. *Lithos* 132–133, 141–161.
- Yakubchuk, A., 2004. Architecture and mineral deposit settings of the Altaiid orogenic collage: a revised model. *Journal of Asian Earth Sciences* 23, 761–779.
- Yang, G.X., Li, Y.J., Gu, P.Y., Yang, B.K., Tong, L.L., Zhang, H.W., 2012. Geochronological and geochemical study of the Darbut Ophiolitic Complex in the West Junggar (NW China): implications for petrogenesis and tectonic evolution. *Gondwana Research* 21, 1037–1049.
- Yin, J.Y., Yuan, C., Sun, M., Long, X.P., Zhao, G.C., Wong, K.P., Geng, H.Y., Cai, K.D., 2010. Late Carboniferous high-Mg dioritic dikes in Western Junggar, NW China: geochemical features, petrogenesis and tectonic implications. *Gondwana Research* 17, 145–152.
- Yogodzinski, G.M., Volynets, O.N., Koloskov, A.V., Seliverstov, N.I., Matvenkov, V.V., 1994. Magnesian andesites and the subduction component in a strongly calc-alkaline series at Piip Volcano, far western Aleutians. *Journal of Petrology* 35, 163–204.
- Yogodzinski, G.M., Kay, R.W., Volynets, O.N., Koloskov, A.V., Kay, S.M., 1995. Magnesium andesite in the western Aleutian Komandorsky region: implications for slab melting and pressures in the mantle wedge. *Geological Society of America Bulletin* 107, 505–519.
- Yogodzinski, G.M., Lees, J.M., Churikova, T.G., Dorendorf, F., Woerner, G., Volynets, O.N., 2001. Geochemical evidence for the melting of subducting oceanic lithosphere at plate edges. *Nature* 409, 500–504.
- Yuan, H.L., Gao, S., Dai, M.N., Zong, C.L., Günther, D., Fontaine, G.H., Liu, X.M., Diwu, C.R., 2007. Simultaneous determinations of U–Pb age, Hf isotopes and trace element compositions of zircon by excimer laser-ablation quadrupole and multiple-collector ICP-MS. *Chemical Geology* 247, 100–118.
- Zhang, Y.Y., Guo, Z.J., 2010. New constraints on formation ages of ophiolites in northern Junggar and comparative study on their connection. *Acta Petrologica Sinica* 26, 421–430 (in Chinese with English abstract).
- Zhang, C., Huang, X., 1992. Age and tectonic settings of ophiolites in west Junggar, Xinjiang. *Geological Review* 38, 509–524 (in Chinese with English abstract).
- Zhang, C., Zhai, M.G., Allen, M.B., Sounders, A.D., Wang, G.R., Huang, X., 1993. Implications of Palaeozoic ophiolites from West Junggar, NW China, for the tectonics of Central Asia. *Journal of the Geological Society (London)* 150, 551–561.
- Zhang, C., Huang, X., Zhai, M.G., 1995. The geological characteristics, tectonic settings and ages of ophiolite in Western Junggar, Xinjiang. *Collected Papers of Institute of Geology*, 8. Chinese Academy of Sciences, Beijing, pp. 165–218 (in Chinese).
- Zhang, H.X., Niu, H.C., Yu, X.Y., Hiroaki, S., Jun'ichi, I., 2003. Discovery of Nb-enriched basalts at the northeast margin of Junggar plate and the geological significance. *Contributions to Geology and Mineral Resources Research* 18, 71–72 (in Chinese with English abstract).
- Zhang, H.X., Niu, H.C., Heroaki, S., Shan, Q., Yu, X.Y., Jun'ichi, I., Zhang, Q., 2004. Late Paleozoic adakite and Nb enriched basalt from Northern Xinjiang: evidence for the southward subduction of the Paleo-Asian Ocean. *Geological Journal of China Universities* 10, 106–113 (in Chinese with English abstract).
- Zhang, H.X., Zhang, B.Y., Niu, H.C., 2005. Partial melting of the slab-derived melt metasomatized mantle peridotite. *Advances in Earth Science* 20, 1234–1242 (in Chinese with English abstract).
- Zhang, L.C., Wan, B., Jiao, X.J., Zhang, R., 2006. Characteristics and geological significance of adakitic rocks in copper-bearing porphyry in Baogutu, western Junggar. *Geology in China* 33, 626–631.
- Zhang, L.F., Ai, Y.L., Li, X.P., Rubatto, D., Song, B., Williams, S., Song, S.G., Ellis, D., Liou, J.G., 2007. Triassic collision of western Tianshan orogenic belt, China: evidence from SHRIMP U–Pb dating of zircon from HP/UHP eclogitic rocks. *Lithos* 96, 266–280.
- Zhang, J.E., Xiao, W.J., Han, C.M., Mao, Q.G., Ao, S.J., Guo, Q.Q., Ma, C., 2011a. A Devonian to Carboniferous intra-oceanic subduction system in Western Junggar, NW China. *Lithos* 125, 592–606.
- Zhang, J.E., Xiao, W.J., Han, C.M., Ao, S.J., Yuan, C., Sun, M., Geng, H.Y., Zhao, G.C., Guo, Q.Q., Ma, C., 2011b. Kinematics and age constraints of deformation in a Late Carboniferous accretionary complex in Western Junggar, NW China. *Gondwana Research* 15, 958–974.
- Zhao, L., He, G.Q., 2013. Tectonic entities connection between West Junggar (NW China) and East Kazakhstan. *Journal of Asian Earth Sciences* 72, 25–32.
- Zhou, L., Wang, X.L., Lei, D.W., Zhang, N.F., He, D.F., Zhang, Y.Q., Zhang, G.Q., Wu, Y., 2006a. Lithology prediction of Upper Carboniferous in Mosuowan uplift in Junggar Basin. *Petroleum Geology* 1, 69–79 (in Chinese with English abstract).
- Zhou, T.F., Yuan, F., Tan, L.G., Fan, Y., Yang, W.P., He, L.X., Yue, S.C., 2006b. Time limit, geochemical characteristics and tectonic setting of late Paleozoic magmatism in Sawuer region, Xinjiang. *Acta Petrologica Sinica* 22, 1225–1237 (in Chinese with English abstract).
- Zhou, T.F., Yuan, F., Fan, Y., Zhang, D.Y., Cooke, D., Zhao, G.C., 2008. Granites in the Saur region of the west Junggar, Xinjiang Province, China: geochronological and geochemical characteristics and their geodynamic significance. *Lithos* 106, 191–206.
- Zhu, B.Q., Feng, Y.M., 1994. Plate tectonics and evolution in west Junggar of Xinjiang. *Xinjiang Geology* 12, 91–105 (in Chinese with English abstract).
- Zhu, Y.F., Xu, X., 2006. The discovery of early Ordovician ophiolite mélange in Taerbahatai Mts., Xinjiang, NW China. *Acta Petrologica Sinica* 22, 2833–2842 (in Chinese with English abstract).
- Zonenshain, L.P., Kuzmin, M.I., Natapov, L.M., 1990. Geology of the USSR: a plate-tectonic synthesis. *Geodynamic Series*, 21. American Geophysical Union, Washington, D.C. (242 pp.).